A NUMERICAL INVESTIGATION OF EXPLOSIVE GENERATED NORMAL MODES AND LEAKING MODES IN AN UNSATURATED SURFACE LAYER OVERLYING A SATURATED HALF-SPACE

Dissertation for the Degree of Ph. D.
MICHIGAN STATE UNIVERSITY
CHING-NAN KAO
1974

This is to certify that the

thesis entitled
A NUMERICAL INVESTIGATION OF EXPLOSIVE GENERATED NORMAL MODES AND LEAKING MODES IN AN UNSATURATED SURFACE LAYER OVERLYING A SATURATED HALF-SPACE

presented by

Ching-nan Kao

has been accepted towards fulfillment
of the requirements for

Ph. D. degree in Geology

Hugh F. Bennett
Major professor

Date 2/25/74

O-7639

A NUMERICAL INVI
WES AND LEAKI
VERLYING A SAT

Most of th
seismograms are
form. The reas
near surface i
earthquake sur
pattern, there
the crust-uppe
to use the hig
wave data fron
geological in
exploration s

A new mo
identified su
M=2, three "p
produced a sm
velocity disp

Some me
found to giv
and Hale's (
that directl

ABSTRACT

A NUMERICAL INVESTIGATION OF EXPLOSIVE GENERATED NORMAL MODES AND LEAKING MODES IN AN UNSATURATED SURFACE LAYER OVERLYING A SATURATED HALF-SPACE

By

Ching-nan Kao

Most of the surface waves recorded on exploration seismograms are characterized by the poorly developed wave form. The reasons are due to short recording distance, near surface inelastic material, etc. On the other hand, earthquake surface waves have a more complete dispersion pattern, therefore, they have long been used to interpret the crust-upper mantle structure. This study is designed to use the high speed computer to process low quality surface wave data from small explosions, in the hope that the geological information contained in the surface waves of exploration seismograms may be better utilized.

A new moving window spectral analysis method successfully identified superimposed modes which included M_{11}, M_{21}, M_{12}, three "pipe organ" type modes, and others. It also produced a smooth time-varying spectrum, from which the group velocity dispersion was determined.

Some methods of computing phase velocities were found to give poor results using available data. Bloch and Hale's (1968) method[1] and a method, developed herein, that directly integrates the observational group velocity

dispersion c

providing go

recorded at

By assu

layer overly

dispersion c

find the mod

were shear w

half-space,

rigidity rat

is to solve

The n non-l

observationa

After severa

phase veloci

averaging the

Another appro

of more than

sum of square

similar resu

The shea

found to be

with the resu

of the surfac

the water tab

increases fro

This is becau

dispersion curve were superior to other methods in providing good phase velocity dispersion curves for data recorded at source distances of 1000 feet and beyond.

By assuming a theoretical model--a single surface layer overlying a infinite half-space, the obtained dispersion curve of the M_{11} mode is then inverted to find the model parameters. The model parameters determined were shear wave velocities in both surface layer and half-space, thickness of the surface layer, and the rigidity ratio of the two layers. One method of inversion is to solve n non-linear equations in the n unknowns. The n non-linear equations are formed by substituting observational phase velocities into the period equation. After several trials using different sets of observational phase velocities, the final solutions are obtained by averaging the results for each trial of n unknowns. Another approach is to solve for n unknowns for a set of more than n non-linear equations by minimizing the sum of squared residues. Both methods have yielded similar results.

The shear wave velocity in the surface layer was found to be 603 feet/second. It is in complete agreement with the result found by direct measurement. The depth of the surface layer of 22 feet is less than the depth to the water table at which the compressional wave velocity increases from 1150 feet/second to 5700 feet/second. This is because normal modes are several times more

sensitive t

compression

was anticip

wave veloci

computed.

A theo

organ type

the water t

completely

multiple of

large source

superior to

depth.

[1]S. Bloch
determinatio
Seism. Soc.

sensitive to the shear wave velocity profile than to compressional wave velocity structure. This result was anticipated. A density ratio of unity and a shear wave velocity for the half-space of 904 feet/second were computed. They were all consistent with known information.

A theoretical interpretation of the dispersive pipe organ type leaking modes was attempted. The depth to the water table, computed by using these modes, agreed completely with the results obtained by using the first multiple of the P head wave from the water table. At large source distances, both methods were found to be superior to the standard refraction technique in computing depth.

[1]S. Bloch and A. L. Hales, New techniques for the determination of surface wave phase velocities, Bull. Seism. Soc. Am., vol. 58, pp. 1021-1034, 1968.

A NUMERICA
NORMAL MOD
SURFACE L

in parti

A NUMERICAL INVESTIGATION OF EXPLOSIVE GENERATED NORMAL MODES AND LEAKING MODES IN AN UNSATURATED SURFACE LAYER OVERLYING A SATURATED HALF-SPACE

By

Ching-nan Kao

A DISSERTATION

Submitted to
Michigan State University
in partial fulfillment of the requirements
for the degree of

DOCTOR OF PHILOSOPHY

Department of Geology

1974

The auth
mbers, Drs.
Carmichael, R
A. Vogel for
It is al
discussions w
of Physics an
Department of

ACKNOWLEDGMENTS

The author is extremely grateful to his guidance committee members, Drs. Hugh F. Bennett (Chairman), Robert S. Carmichael, Robert Ehrlich, Charles M. Spooner, and Thomas A. Vogel for their guidance and encouragement.

It is also a pleasure to acknowledge several helpful discussions with Dr. Wayne W. Repko of the Department of Physics and Astronomy and Dr. James F. Hannan of the Department of Statistics and Probability.

TABLE OF CONTENTS

Table

LIST OF TABLES

Figure

1. Layered
2. A Porti
3. Time-va (Recc
4. Events (Recc
5. Events (Recc
6. Time-va 43, S
7. Observa
8. Amplitu
9. Amplitu
10. Determi
11. Phase V
12. An Exam
13. Trapezo
14. A Small Varyi
15. Phase V Fouri No. 4
16. Observe Mode

LIST OF FIGURES

Normal a
subsurface ge
Because the b
simple geomet
seismic inter
leaking modes
simple theori
puter, the su
tremendously
mining the th
ties of crust
last two deca

The surf
been widely u
usually recor
fore, the sur
addition, the
the material
assume a corr
exploration s
surface wave
techniques a
of the surfa
explosion.

Chapter I
Introduction

Normal and leaking mode seismic surface waves contain subsurface geological information as do the body waves. Because the body waves, in most cases, are predictable by simple geometrical ray theory, they have long been used in seismic interpretation. On the other hand, normal modes, leaking modes, diffraction, etc. cannot be described by simple theories. Since the advance of the high-speed computer, the surface wave solution computing time has been tremendously reduced. The use of surface waves in determining the thickness of the crust and the physical properties of crust and upper mantle has become popular in the last two decades.

The surface waves from a small explosion have not yet been widely utilized in seismic interpretation. They are usually recorded at short distances from the source, therefore, the surface waves are usually not well developed. In addition, the near surface heterogeneity and departure of the material from perfect elasticity makes it difficult to assume a correct theoretical model. These facts inhibit the exploration seismologist from making practical use of the surface wave. Our study aims at improving the available techniques and developing new methods in order to make use of the surface wave normal and leaking modes from a small explosion.

The grou

cle motion, a

surface wave.

can determine

Two meth

city dispersi

city by divi

ing time of a

by inspectio

This is a tra

persion. An

sis techniqu

(1969), but

method. The

the one used

The pha

many differe

Hales (1968)

a smoother c

velocities b

cities. The

previous met

we had tried

due to the s

details of v

The ref

supplied by

The group velocity and phase velocity dispersion, particle motion, and amplitude spectrum are characteristic of a surface wave. They must be correctly computed before one can determine the corresponding earth model.

Two methods have been used to calculate the group velocity dispersion curve. One is to determine the group velocity by dividing the distance to the station by the arriving time of a particular period. Measurement of the period by inspection is valid only when a single mode is present. This is a traditional method of deriving group velocity dispersion. Another method is the moving window spectral analysis technique. It is similar to Landisman, et al.'s method (1969), but was developed without prior knowledge of his method. There are some differences between his method and the one used here as will be explained in Chapter III.

The phase velocity dispersion can be determined using many different approaches. A method first used by Bloch and Hales (1968) obtained a good result. As an attempt to find a smoother curve, a method was developed to derive the phase velocities by direct integration of the observed group velocities. The results obtained were in agreement with the previous method of Bloch and Hales. Several other methods we had tried did not yield usable results. It was apparently due to the short time duration of signals and noises. The details of various methods will be discussed in Chapter IV.

The refraction records used in this study were kindly supplied by Dr. H. F. Bennett of the Department of Geology.

A total of 24
the first 8 t
otion. The
ransverse mo
ertical moti
ent geophone
phones used w
of the record
ties. The na
and the dampi
response was
used were rec
settings. Ba

A digiti
tize the reco
interval was
frequency of
study were we
Hertz).

The reco
Manistee Coun
cording area
correction, t

This are
glacial drift
clay. The un
shale layers

A total of 24 traces were recorded on photographic paper. The first 8 traces were X component or horizontal in-line motion. The second 8 traces were Y component or horizontal transverse motion. The third 8 traces were Z component or vertical motion. At each detection position, a three component geophone recorded the X, Y, and Z motions. The geophones used were of the moving coil type. The amplitudes of the recordings were proportional to the particle velocities. The natural frequency of the geophones was 4.5 Hertz and the damping was 62% of the critical frequency. The response was essentially flat above 7 Hertz. All the data used were recorded without Automatic Gain Control and filter settings. Bandpass was therefore about 7 to 125 Hertz.

A digitizer owned by the University was used to digitize the records for use on digital computer. The digitizing interval was 0.005 sec. which corresponded to the Nyquist frequency of 100 Hertz. The frequencies encountered in this study were well below the Nyquist frequency (i.e., 10-50 Hertz).

The records were recorded in the Udell Hills area of Manistee County, Michigan. The ground surface in the recording area is essentially horizontal. The topographic correction, therefore, was not necessary.

This area contains approximately 500 ft. of Pleistocene glacial drift. It is composed mainly of sand with strips of clay. The underlying formation contains sandstone with some shale layers which is of Mississippian age. The water table

at the locati

at a depth of

description o

Todd (1971).

In study

corresponding

chosen before

shear wave ve

selecting a m

btained by c

distance curv

as a marked c

The critical

rated layer

table and the

energy trappe

Therefore, we

records take

are the trans

guide. Thro

be assumed.

in Ewing, et

A probl

interface of

more sensiti

whereas the

city distrib

an increase

at the location where the records were obtained was located at a depth of about 32 ft. below the surface. A detailed description of the geology of this area can be found in Todd (1971).

In studying surface waves, a particular period equation corresponding to a particular theoretical model must be chosen before the study proceeds. The compressional and shear wave velocity distribution in this area is vital in selecting a model. Table 1 is a list of body wave velocities obtained by direct measurements and from refraction time-distance curves. It is observed that the water-table acts as a marked discontinuity for compressional wave velocity. The critical angle of the compressional wave in the unsaturated layer is about 11½°. If all shots were above water-table and the shear waves were not taken into account, the energy trapped in the surface layer would be about 98%. Therefore, we expect the prominent feature of the seismic records taken in this area to be composed of signals that are the transient response of the surface unsaturated wave guide. Through this study, a single surface layer model will be assumed. The period equation for this model can be found in Ewing, et al.(1957, pp. 193).

A problem exists in assuming the water-table to be the interface of our single layer model. The leaking mode is more sensitive to the compressional velocity distribution, whereas the normal mode is more sensitive to the shear velocity distribution (Su and Dorman, 1965, p. 1018). In general, an increase in compressional velocity accompanies an increase

Table 1. Bod

Compressional
Wave Velocity
(ft/sec)

Shear Wave
Velocity
(ft/sec)

† Obtained
* Obtained

Table 1. Body Wave Distribution in Udell Hills Area

	Unsaturated Glacial Drift	Saturated Glacial Drift	Mississippian S.S.
Compressional Wave Velocity (ft/sec)	#1150	*5700	*13461
Shear Wave Velocity (ft/sec)	# 600	?	?

Obtained by direct measurements
* Obtained by time-distance curves

in shear velo

sure that the

below the wat

shear velocit

level. This

Dobrin, et al

Mann, 1960) h

the experimen

increase belo

to accept or

to assume tha

table is smal

velocity. If

changes due t

tude than the

assumed a sin

face, found b

different for

surface-layer

In Chapter II

leaking mode

Compress

(S-wave) velo

of any two ad

characterizin

cities and th

metrical ray

in shear velocity. In this particular case, we can be sure that the compressional velocity increases greatly below the water-table, but we hesitate to infer that the shear velocity also increases substantially at the same level. This is because several papers (Biot, 1956a, 1956b; Dobrin, et al, 1954; Ewing, et al, 1957; Kisslinger, 1959; Mann, 1960) have reported, using either the theoretical or the experimental basis, that the shear velocity does not increase below the water-table. There is no solid ground to accept or to reject their finding, but it may be safe to assume that the change in shear velocity at the water-table is small as compared to the change in compressional velocity. If this assumption is true, the shear velocity changes due to the clay layers is possibly of greater magnitude than the change at the water-table. Because we have assumed a single surface layer model, the depth to the interface, found by the inversion of the observed data, may be different for normal and leaking modes. However, the single surface-layer model will still be used through the study. In Chapter II, we will make a theoretical treatment of the leaking mode based upon the above assumption.

Compressional wave (P-wave) velocities, shear wave (S-wave) velocities, thickness of layers, and rigidity ratio of any two adjacent layers are important parameters in characterizing a horizontal stratified model. Body wave velocities and thicknesses are possibly deduced by a simple geometrical ray theory. The rigidity ratios and their dependent

parameters (

only be found

Two meth

phase velocit

methods are

in Chapter V

develop a le

data. They

sum of squar

the true pha

also lineari

study solve

computer. O

for least-sq

squared resi

development

ledge of the

methods of t

the results

The bes

sion methods

substituting

equation of

correctness

sulting phas

The res

provide an i

parameters (i.e., density ratio and Poisson's ratios) can only be found by using surface wave data.

Two methods were developed to inverse the observed phase velocity dispersion data. The results from both methods are in good agreement. The details will be given in Chapter V. Dorman and Ewing (1962) were the first to develop a least-square technique to invert the surface wave data. They derived the normal equations by minimizing the sum of squared errors which were the differences between the true phase velocity and the assumed phase velocity. They also linearized the entire process. The methods in this study solve a system of non-linear equations directly on the computer. One solves for exact solutions and another solves for least-square solutions by minimizing the sum of the squared residues of the period equation. As before, the development of these methods were accomplished without knowledge of the one explained by Dorman and Ewing (1962). The methods of this study will not be compared to theirs, but the results are expected to be in agreement.

The best method to check the correctness of the inversion methods described above is to reverse the process. By substituting the model parameters obtained into the period equation of the assumed theoretical model, one can check the correctness of the inversion methods by comparing the resulting phase and group velocities with the observed data.

The results of the surface wave computation not only provide an independent check on the information extracted

from the body

cerning the ph

which are usua

tions in these

the high-speed

siderably lowe

use of the sur

tion, uncerta

termine local

still has som

body waves on

from the body wave data, but also gives more information concerning the physical properties of the subsurface layers which are usually not provided by body waves. The calculations in these processes are laborious, but with the aid of the high-speed computer, the time and cost have been considerably lowered. Despite the intrinsic drawbacks of the use of the surface wave data, such as the limited penetration, uncertainty in determining layering, inability to determine localized structure, etc., the use of surface waves still has some advantages that cannot be surmounted by using body waves only.

A sinc

Figure 1.

denote the

respective

layer i

with thick

depth B an

depth b

such as:

$$u = \mathrm{Re}\left\{ \int_{-\infty}^{\infty} e \right.$$

where Re d

w =

k =

C =

Jo

Q =

P =

j =

Evaluatio

Chapter II
Theory

A single layer over a half-space model is shown in Figure 1. The symbols α_i , β_i , and ρ_i in the figure denote the P wave velocity, S wave velocity, and density respectively, where the subscript i corresponds to the layer i . The transient response of the surface layer with thickness h for any component of the motion u , at depth z and distance r from an impulse point source at depth b is given by a double integral (Ewing, et al, 1957) such as:

$$u = \mathrm{Re}\int_{-\infty}^{\infty} \exp(jwt)\,dw \int_{-\infty}^{\infty} \frac{Q(w,k,z,b)J_o(kr)\,dk}{P(w,k)} \quad \text{.....(2.1)}$$

where Re denotes the real part of the double integral

w = angular frequency

k = wave number = w/C

C = Phase velocity

Jo = the Bessel function of zero order

Q = a function of w, k, z, and b

P = a function of w and k

$j = \sqrt{-1}$.

Evaluation of this double integral can be performed in several

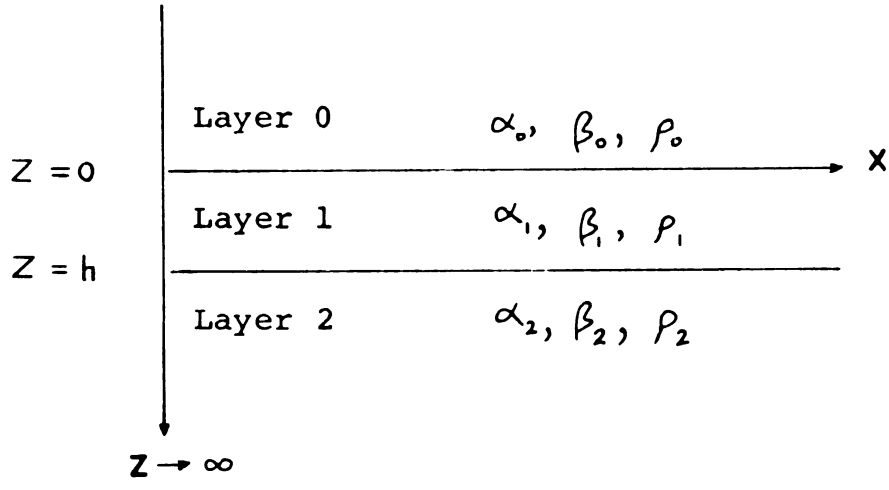

Figure 1. Layered Model

ways. One
Cauchy's th
method of s
spectral pr
the integra
solution is
and the bra
which may b
variables,
able. The

A. Ph

The ve
velocity.
as A exp(
w,k,t, and
ing without
ment wt-kr

wt - kdr

For a
group velo
Suppose a
number of
it may be

u(x,t)

ways. One method is to integrate the inner integral by Cauchy's theorem on the complex plane and the other by the method of stationary phase. Since we are interested in the spectral properties of the transient response, only one of the integrals has to be solved. The contribution to the solution is from the poles within the contour of integration and the branch lines. The poles are the zeros to P (w,k) which may be real or complex. Note that P (w,k) has two variables, w and k, the zeros being functions in one variable. The locus of a zero is the dispersion curve of a mode.

A. Phase Velocity and Group Velocity

The velocity of wave propagation is called the phase velocity. Assume that a propagating wave is expressible as $A \exp(j(wt-kr))$, where A is the amplitude and w,k,t, and r are defined as before. For this wave, traveling without continuously changing its wave form, the argument wt-kr must be kept constant. This requirement leads to:

$$wdt - kdr = 0 \quad \text{or} \quad C = dr/dt = w/k = \text{Phase velocity} \ldots\ldots (2.2)$$

For a dispersive wave train, there is a velocity called group velocity U which is different from the phase velocity. Suppose a wave is made up of superposition of an infinite number of waves with continuously changing wave number k. It may be expressed as:

$$u(x,t) = \int_{-\infty}^{\infty} A(k) \exp(j(w(k)t-kr)) \, dk \ldots\ldots\ldots\ldots\ldots (2.3)$$

The conc

A(k) whi

particul

small fo

the wave

$u(x,t)$

By expan

$w(k) =$

and negl

$u(x,t)$

where f(

The quar

tude of

leads to

$f(k,r,t$

for the

associat

The concept of group velocity applies only to those cases A(k) which have a significant value in the neighborhood of a particular wave number, say ka, and becomes vanishingly small for k outside a small range, denoted by $k_a \pm \Delta k$. Then, the wave function can be written approximately as:

$$u(x,t) = \int_{k_a-\Delta k}^{k_a+\Delta k} A(k)\, \exp(j(w(k)t - kr))\, dk \quad \ldots\ldots\ldots\ldots (2.4)$$

By expanding w(k) about $k = k_a$,

$$w(k) = w(k_a) + (dw/dk)_{k=k_a}(k - k_a) + \ldots\ldots\ldots$$

and neglecting higher order terms, equation (2,4) becomes

$$u(x,t) = \int_{k_a-\Delta k}^{k_a+\Delta k} A(k)\, \exp(jf(k,r,t))\, \exp(jg(r,t))\, dk, \quad \ldots (2.5)$$

where $f(k,r,t) = (k-k_a)\left(\frac{dw}{dk}_{k=k_a} t - r\right)$ and $g(r,t) = w(k_a)t - k_a r$. The quantity $A(k)\exp(jf(k,r,t))$ is the effective amplitude of the wave. The requirement of constant phase now leads to

$$f(k,r,t) = 0 \quad \text{or} \quad (dw/dk)_{k=k_a} = r/t = u \quad \ldots\ldots\ldots\ldots (2.6)$$

for the group velocity. Thus the energy of a wave, which is associated with the amplitude, travels with the group velocity

r. Equa

$v = (C/$

where k_a

C = cons

B.

The

tion whi

A form o

ence (E

computa

where

U. Equation (2.6) can be rewritten as:

$$U = \left(C/\left(1 - \frac{w}{C}\frac{dC}{dw}\right)\right)_{w=w_a} \text{ and } C=C_a \quad \ldots\ldots\ldots\ldots\ldots\ldots (2.7)$$

where $k_a = w_a/C_a$. For a dispersive wave train, C = constant or dC/dw = 0 hence $U = C_a$.

B. Period Equation

The denominator of equation (2.1) is the period equation which determines the dispersion pattern of the model. A form convenient for computation is given below for reference (Ewing, et al, p. 193). We will use this form for computation throughout the study.

$$\xi_1 \eta_2 - \xi_2 \eta_1 = 0 \quad \ldots\ldots\ldots\ldots\ldots\ldots\ldots\ldots (2.8)$$

$$\begin{aligned}
\text{where } \xi_1 &= \left(2 - \frac{k^2\beta_1^2}{k^2}\right)\left(X \cos r_1 h + \frac{r_2}{r_1} Y \sin r_1 h\right) \\
&\quad + 2\frac{s_1}{k}\left(\frac{r_2}{k} W \sin s_1 h - \frac{k}{s_1} Z \cos s_1 h\right) \\
\xi_2 &= \left(2 - \frac{k^2\beta_1^2}{k^2}\right)\left(\frac{s_2}{k} W \cos r_1 h + \frac{k}{r_1} Z \sin r_1 h\right) \\
&\quad + 2\frac{s_1}{k}\left(X \sin s_1 h - \frac{s_2}{s_1} Y \cos s_1 h\right) \\
\eta_1 &= \left(2 - \frac{k^2\beta_1^2}{k^2}\right)\left(\frac{r_2}{k} W \cos s_1 h + \frac{k}{s_1} Z \sin s_1 h\right) \\
&\quad + 2\frac{r_1}{k}\left(X \sin r_1 h - \frac{r_2}{r_1} Y \cos r_1 h\right) \\
\eta_2 &= \left(2 - \frac{k^2\beta_1^2}{k^2}\right)\left(X \cos s_1 h + \frac{s_2}{s_1} Y \sin s_1 h\right) \\
&\quad + 2\frac{r_1}{k}\left(\frac{s_2}{k} W \sin r_1 h - \frac{k}{r_1} Z \cos r_1 h\right)
\end{aligned} \quad \ldots\ldots (2.9)$$

$$\lambda = \frac{\mu_2}{\mu_1}\frac{k\beta_2^2}{k^2}$$

$$\gamma = \frac{\mu_2}{\mu_1}\frac{k\beta_2^2}{k^2}$$

$$r_1^2 = k_{\alpha_1}^2 -$$

$$s_1^2 = k_{\beta_1}^2 -$$

μ_1 = rig

f = fre

α_1 = com

β_1 = she

k_{α_1} = $\frac{2}{}$

k_{β_1} = $\frac{2}{}$

A differe

given by

$|N-M^{-1}|$

$$X = \frac{\mu_2}{\mu_1}\frac{k_{\beta_2}^2}{k^2} - 2\left(\frac{\mu_2}{\mu_1} - 1\right) \qquad Y = \frac{k_{\beta_1}^2}{k^2} + 2\left(\frac{\mu_2}{\mu_1} - 1\right)$$

$$Z = \frac{\mu_2}{\mu_1}\frac{k_{\beta_2}^2}{k^2} - \frac{k_{\beta_1}^2}{k^2} - 2\left(\frac{\mu_2}{\mu_1} - 1\right) \qquad W = 2\left(\frac{\mu_2}{\mu_1} - 1\right) \qquad \text{.....(2.10)}$$

$$r_1^2 = k_{\alpha_1}^2 - k^2 \qquad r_2^2 = k^2 - k_{\alpha_2}^2$$

$$s_1^2 = k_{\beta_1}^2 - k^2 \qquad s_2^2 = k^2 - k_{\beta_2}^2 \qquad \text{.....(2.11)}$$

μ_i = rigidity of the layer i

f = frequency

α_i = compressional wave velocity in the layer i

β_i = shear wave velocity in the layer i

$$k_{\alpha_i} = \frac{2\pi f}{\alpha_i}$$

$$k_{\beta_i} = \frac{2\pi f}{\beta_i}.$$

A different form of the period equation of a wave guide is given by Tolstoy and Usdin (1953) as follows:

$$\left| N - M^{-1} \right| = 0 \qquad \text{.....(2.12)}$$

where |

$$N = \begin{vmatrix} A\ ex \\ B\ ex \end{vmatrix}$$

$$M = \begin{vmatrix} G\ ex \\ H\ ex \end{vmatrix}$$

$$M^{-1} = \frac{1}{|M|}$$

A,B,C, and

SS respect

efficients

Comir

asymptotic

pp. 193-19

obtained w

shown tha

zero, equa

tion for

(i.e., hi

becomes f

Rayleigh

zero of t

interface

As T

where $|\ \ |$ denotes the determinant

$$N = \begin{pmatrix} A\exp(jr_1h) & C\exp(jr_1h) \\ B\exp(js_1h) & D\exp(js_1h) \end{pmatrix} \quad \ldots\ldots\ldots\ldots\ldots\ldots \quad (2.13)$$

$$M = \begin{pmatrix} G\exp(jr_1h) & J\exp(jr_1h) \\ H\exp(js_1h) & I\exp(js_1h) \end{pmatrix} \quad \ldots\ldots\ldots\ldots\ldots\ldots \quad (2.14)$$

$$M^{-1} = \frac{1}{|M|} \begin{pmatrix} I\exp(js_1h) & J\exp(jr_1h) \\ -H\exp(js_1h) & G\exp(jr_1h) \end{pmatrix} = \text{inverse of } M. \quad (2.15$$

A,B,C, and D are reflection coefficients of PP, PS, SP, and SS respectively at $z=0$. G,H,J, and I are reflection coefficients of PP, PS, SP, and SS respectively at $z = h$.

1. Normal Mode Roots of Period Equation

Coming back to equation (2.8), let us discuss some asymptotic roots of this equation (Ewing, et al, 1957, pp. 193-196). Positive real values of s_i, r_i are obtained when $C > \alpha_1 > \beta_1$ and $C < \beta_2 < \alpha_2$. It can be shown that when the thickness of the layer h approaches zero, equation (2.8) becomes the simple Rayleigh wave equation for the half-space. For $C < \beta_1$ and $kh \to \infty$, (i.e., high frequencies) the asymptotic form of equation (2.8) becomes factorable. The zero of the first factor represents Rayleigh waves at the upper surface of the layer, while the zero of the second factor represents Stoneley waves at the interface.

As Tolstoy and Usdin (1953) have shown, there are two

branches

$w_{12},\ldots)$

these ar

rvely.

Tolstoy

the phas

of the h

velocity

layer.

dicate t

of half-

shear wa

limit.

termed s

shear mo

low whic

In

(1953),

uncondi-

a solid

a vacuu

Tolstoy

$D = -A$

$G = \Gamma$

$H = \Lambda$

branches of zeros that exist. One is the M_1 branch (M_{11}, M_{12},...) and another is the M_2 branch (M_{21}, M_{22},...). These are also termed symmetric and antisymmetric, respectively. Some interesting features may be found in Figure 10, Tolstoy and Usdin (1953), p. 860. At long wave limits $kh \to 0$, the phase velocity of M_{11} approaches Rayleigh wave velocity of the half-space and at short wave limits $kh \to \infty$, this velocity approaches the Rayleigh wave velocity of the surface layer. All other modes, including M_{21}, M_{12}, M_{22}, etc. indicate that phase velocity approaches the shear wave velocity of half-space at the long wave limit and approaches the shear wave velocity of the surface layer at the short wave limit. This is why Rayleigh modes, except the M_{11} mode, are termed shear modes (Mooney and Bolt, 1966, p. 45). All shear modes have cutoff frequencies at long wave limits, below which no unattenuated propagations can occur.

In addition to the conclusions of Tolstoy and Usdin (1953), it is demonstrated below that two branches, M_1 and M_2, unconditionally, exist in the solid surface layer overlying a solid half-space. By referring to Figure 1, layer 0 is a vacuum, $\alpha_0 = \beta_0 = \rho_0 = 0$. Some useful relations according to Tolstoy and Usdin are:

$$D = -A \qquad A^2 + BC = 1 \qquad \text{.....(2.16)}$$

$$G = \Gamma \exp[-j(\epsilon + \bar{\epsilon})] \qquad J = \frac{r_1 s_1}{k^2} \wedge \exp(-j\epsilon)$$
$$H = \wedge \exp(-j\epsilon) \qquad I = -\Gamma \exp[-j(\epsilon - \bar{\epsilon})] \qquad \text{....(2.17)}$$

where Γ

Also, -

-

and -

It can

GI - HJ

Γ^2 + Λ

and at

C = $\frac{\Gamma}{k}$

BJ = B

The per

-exp [j

+ AΓ (e

+ 2 $\frac{\Gamma}{k}$

Equatio

and Usd

Cos[(r_1

where Γ is real and positive, and Λ is real for normal modes.

Also, $-(\epsilon + \bar{\epsilon})$ is the phase shift of PP at $\zeta = h$,

$-\epsilon$ is the phase shift of PS and SP at $\zeta = h$,

and $-(\epsilon - \bar{\epsilon}) - \pi$ is the phase shift of SS at $\zeta = h$.

It can also be shown that at $\zeta = h$

$$GI - HJ = -\exp(-2j\epsilon) \quad \text{..... (2.18)}$$

$$\Gamma^2 + \Lambda^2 \frac{r_1 s_1}{k^2} = 1, \quad \text{..... (2.19)}$$

and at $\zeta = o$

$$C = \frac{r_1 s_1}{k^2} B \quad \text{..... (2.20)}$$

$$BJ = B \frac{r_1 s_1}{k^2} \Lambda \exp(-j\epsilon) = C\Lambda \exp(-j\epsilon) = CH \quad \text{..... (2.21)}$$

The period equation (2.12) can be written as

$$-\exp[j(r_1+s_1)h - j\epsilon] \exp[j(r_1+s_1)h + j\epsilon]$$
$$+ A\Gamma(\exp[j(r_1-s_1)h - \bar{\epsilon}j] + \exp[-j(r_1-s_1)h + \epsilon j]$$
$$+ 2 \frac{r_1 s_1}{k^2} B\Lambda = o \quad \text{..... (2.22)}$$

Equation (2.22) can be rewritten as the form shown in Tolstoy and Usdin (1953) p. 859:

$$\cos[(r_1 + s_1)h - \epsilon] - A\Gamma \cos[(r_1 - s_1)h - \bar{\epsilon}] = C\Lambda \quad \text{..... (2.23)}$$

It can also be written as:

$$S^2 = T + Q/2 \qquad (2.24)$$

where $S = \sin\left[\frac{(r_1+s_1)h - \epsilon}{2}\right]$

$T = A \sin^2\left[\frac{(r_1-s_1)h - \bar{\epsilon}}{2}\right]$

$Q = 1 - \frac{r_1 s_1}{k^2} B\Lambda - A\Gamma$.

Since all the quantities in this equation are real, the left hand side is always positive and less than or equal to one. By equations (2.19) and (2.16), the first term on the right, T, is also positive and less than or equal to one under all conditions. The derivation of the M_1 and M_2 branches is arrived at by factoring equation (2.24)

$$[S-(T + Q/2)^{1/2}] [S + (T + Q/2)^{1/2}] = o \qquad (2.25)$$

which leads to the equation on p. 860, Tolstoy and Usdin (1953). The factoring requires that $(T+Q/2)^{1/2}$ be real, or the equivalence, (T+Q/2) be positive. As we have seen previously, T is always positive in normal mode case. If one is able to prove that Q is also positive under same conditions the quantity (T+Q/2) will be automatically positive, hence, the factoring in equation (2.25) will be legal. In the following we will prove that Q is positive in normal mode case: In normal mode case, A, B, Λ , and Γ are real quantities and r_1, s_1, and k^2 are real and positive.

Therefore, the expression

$$\frac{r_1 s_1}{k^2}(A\Lambda - B\Gamma)^2 \geq 0 \qquad (2.26)$$

is no doubt true. By expanding the inequality (2.26) and adding $(\frac{r_1 s_1}{k^2})^2 B^2\Lambda^2 + A^2\Gamma^2$ to both sides of the inequality, we obtain

$$(\frac{r_1 s_1}{k^2})^2 B^2\Lambda^2 + A^2\Gamma^2 + 2\frac{r_1 s_1}{k^2} B\Lambda A\Gamma \leq (\frac{r_1 s_1}{k^2})^2 B^2\Lambda^2 + A^2\Gamma^2 + \frac{r_1 s_1}{k^2}(A^2\Lambda^2 + B^2\Gamma^2)$$

or

$$(\frac{r_1 s_1}{k^2} B\Lambda + A\Gamma)^2 \leq (\frac{r_1 s_1}{k^2}\Lambda^2 + \Gamma^2)(\frac{r_1 s_1}{k^2}B^2 + A^2) \qquad (2.27)$$

The right hand side of the inequality (2.27) is equal one by using equation (2.16), (2.20) and equation (2.19). Hence the inequality (2.27) becomes

$$(\frac{r_1 s_1}{k^2} B\Lambda + A\Gamma) \leq 1$$

or

$$-1 \leq \frac{r_1 s_1}{k^2} B\Lambda + A\Gamma \leq +1,$$

namely,

$$Q = 1 - \frac{r_1 s_1}{k^2} B\Lambda - A\Gamma \geq 0 \qquad (2.28)$$

The quantity on the left hand side of the inequality (2.28) is just the quantity Q defined in equation (2.25). The proof is complete.

2. Leaking Mode Roots of Period Equation

In studying the leaking and the normal mode roots of the period equation there are two simplified approaches that are convenient for discussion. Gilbert (1964) assumes wave number k to be real and frequency f to be complex while Watson (1972) assumes the opposite. Alsop (1970) shows that both approaches are valid.

Gilbert's (1964) method has been widely quoted. He proceeds by first finding the initial position of each root at k=0 and then by following each root as k increases, thereby generating dispersion curves. For k=0 and f finite, i.e., phase velocity $C \rightarrow \infty$, or at normal incidence, the period equation becomes the product of two factors. The roots to each factor are shear pipe organ modes and compressional pipe organ modes. When k increases from zero, these roots gradually change their properties and split into two or more roots. Some roots finally become the higher order shear modes. He also shows that if $k \rightarrow o$ and $f \rightarrow o$ such that f/k is finite, the period equation becomes proportional to the Rayleigh's equation of the half-space. Due to the presence of the radicals

$$r_2 = (k^2 - k_{\alpha 2}^2)^{1/2} \quad \text{and} \quad s_2 = (k^2 - k_{\beta 2}^2)^{1/2}$$

there are two pairs of branch points, $f = \pm \frac{C}{2\pi} k_{\alpha 2}$ and $f = \pm \frac{C}{2\pi} k_{\beta 2}$, on complex f plane. The Riemann sheets are formed according to Re $r_2 > 0$ and Re $s_2 > 0$, Re $r_2 < 0$ and Re $s_2 < 0$, Re $r_2 > o$ and Re $s_2 < 0$, and Re $r_2 < 0$ and Re $s_2 > o$.

bif

The

int

S w

tra

are

Re

and

bra

Pay

pip

mod

the

liq

(li

lgs

app

pro

tic

pea

(E

bee

in

Different Riemann sheets have different groups of roots. The roots on different sheets have different physical interpretations. For example, Re $s_2 < o$ means leaking of S wave energy into the half-space, and Re $r_2 > o$ means trapping of P wave energy in the surface layer.

The roots of this equation according to Gilbert (1964) are: $\bar{S}$ roots on the Riemann sheet (+,+) (i.e., Re $r_2 > o$, Re $s_2 > o$) and (-,-) (i.e., Re $r_2 < 0$, Re $s_2 < 0$) and $\bar{P}$ roots on (+,-) and (-,+) sheets. $\bar{S}$ roots eventually become M_1 branch of Rayleigh waves and $\bar{P}$ roots become M_2 branch of Rayleigh waves. The $\bar{P}$ +- and $\bar{P}$-+ , compressional and shear pipe organ modes, respectively (not the true "pipe organ" modes) have been identified on earthquake seismograms.

The leaking modes found in our data are similar to the normal mode propagation in a liquid layer overlying a liquid half-space in which only P waves enter the problem (liquid cannot sustain the shear motion) (Ewing, et al, 1957, pp. 126-151; Officer, 1958, pp. 117-145). When C approaches α_2 , or equivalently the incident angle approaches normal, the normal mode equation becomes the equation for the simple pipe organ modes whose spectral band peaks at 1, 3, 5, --- times the fundamental frequency (Ewing, et al, 1957, p. 185). This phenomenon has also been reported by Grant and West (1965, pp. 104-107).

It is strange to see that the above phenomenon exists in the solid layer overlying a solid half-space, because in

solids, both P and S waves in the general case couple to each other at the interfaces. Two possible explanations are discussed here. One explanation may be decoupling of P waves and S waves due to their high angle of emergence in the surface layer. The critical angle of the P wave in the layer is 11° 34' and the shear wave generated by the compressional wave impinging at the boundaries has an incident angle of 6° 00'. Both are small. Another explanation is based upon the assumption that the reflected S wave from water-table has small amplitude because of the small S wave velocity discontinuity at the saturated-unsaturated boundary, which has already been discussed in some detail in Chapter I. It is difficult to determine which explanation is correct. At near normal incidence, impinging SV waves generate neglegible amplitudes of the reflected P waves at a boundary, but the impinging P waves generate about equal amplitudes of reflected P waves and S waves (Muskat and Meres, 1940). This infers that X component amplitudes must be similar in magnitude to the Z component after the arrival of α_2 . This is not the case we have observed on our records. It is observed that the X component traces have smaller amplitudes than the Z component traces after the arrival of the refracted α_2. A portion of record No. 43 is shown in Figure 2. However, we still have grounds to argue that since S wave energy is more easily dissipated in the near surface loose material, the amplitudes of S wave shown on the seismograms are more severely attenuated than the amplitudes of P wave.

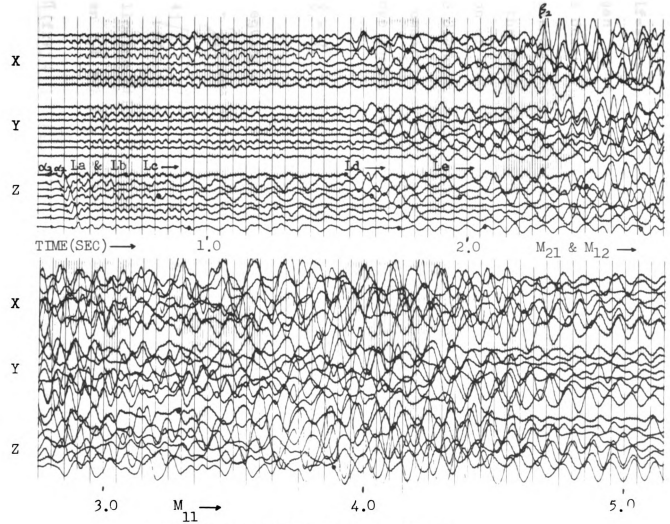

FIGURE 2. A PORTION OF RECORD NO. 43

If the S wave velocity change at the water-table is assumed to be small and the density change is also assumed to be not substantial, an interesting result can be derived from the period equation of the single surface layer over a half-space model. The existence of the dispersive "pipe organ" modes in the assumed earth model is then explainable. The derivation is made possible by simplifying the period equation under the assumptions: $\beta_1 = \beta_2$ and $\rho_1 = \rho_2$. In the following, we want to show that the normal mode equation of the liquid layers is a possible equation governing the dispersion pattern of the leaking modes propagating in an unsaturated layer overlying a saturated half-space if the above assumptions are true. By substituting

$$\beta_1 = \beta_2, \quad \mu_1 = \mu_2 \text{ , and } \rho_1 = \rho_2$$

in equation (2.8), it becomes

$$(2 - \frac{C^2}{\beta_1^2})[\cos(r_1 h) + \frac{r_2}{r_1} \sin(r_1 h)]$$

$$+ 4j\sqrt{\frac{C^2}{\beta_1^2} - 1}\sqrt{\frac{C^2}{\alpha_1^2} - 1}\,[\frac{r_2}{r_1}\cos(r_1 h) - \sin(r_1 h)] = 0 \ldots\ldots\ldots (2.30)$$

Following Gilbert's (1964) method, we assume $f = f_r + j f_i$, then $r_1 h = k\sqrt{\frac{C^2}{\alpha_1^2} - 1}\, h = \frac{2\pi f}{C}\sqrt{\frac{C^2}{\alpha_1^2} - 1}\, h =$

$\frac{2\pi(f_r + j f_i)}{C}\sqrt{\frac{C^2}{\alpha_1^2} - 1}\, h = R + jI$. Equation (2.30) can be written as:

$$\Pi_1 \Sigma_1 + j \Pi_2 \Sigma_2 = 0 \quad \ldots\ldots\ldots\ldots\ldots\ldots\ldots\ldots \quad (2.31)$$

where

$$\Pi_1 = (2 - \frac{C^2}{\beta_1^2})^2 \text{ Cosh (I)} + 4\sqrt{\frac{C^2}{\beta_1^2} - 1}\ \sqrt{\frac{C^2}{\alpha_1^2} - 1}\ \text{sinh (I)} \quad \ldots\ldots \quad (2.32a)$$

$$\Sigma_1 = \text{Cos (R)} + \frac{\sqrt{1 - C^2/\alpha_2^2}}{\sqrt{C^2/\alpha_1^2 - 1}}\ \text{sin (R)} \quad \ldots\ldots\ldots\ldots\ldots\ldots \quad (2.32b)$$

$$\Pi_2 = (2 - \frac{C^2}{\beta_1^2})\ \text{sinh (I)} + 4\sqrt{\frac{C^2}{\beta_1^2} - 1}\ \sqrt{\frac{C^2}{\alpha_1^2} - 1}\ \text{Cosh (I)} \quad \ldots \quad (2.32c)$$

$$\Sigma_2 = \frac{\sqrt{1 - C^2/\alpha_2^2}}{\sqrt{C^2/\alpha_1^2 - 1}}\ \text{Cos (R)} - \text{sin (R)} \quad \ldots\ldots\ldots\ldots\ldots\ldots \quad (2.32d)$$

For equation (2.31) to be satisfied, four possible branches of roots can be solved from the four sets of equations listed below:

$$\Pi_1 = 0 \quad \text{and} \quad \Pi_2 = 0 \quad \ldots\ldots\ldots \quad (2.33a)$$

$$\Pi_1 = 0 \quad \text{and} \quad \Sigma_2 = 0 \quad \ldots\ldots\ldots \quad (2.33b)$$

$$\Sigma_1 = 0 \quad \text{and} \quad \Pi_2 = 0 \quad \ldots\ldots\ldots \quad (2.33c)$$

$$\Sigma_1 = 0 \quad \text{and} \quad \Sigma_2 = 0 \quad \ldots\ldots\ldots \quad (2.33d)$$

These equations may or may not have solutions. Equation (2.33c) can be explicity written as

$$\tanh\left(\frac{2\pi f_i h}{\alpha_1} \text{Cos } \theta\right) = -\frac{4\sqrt{C^2/\beta_1^2 - 1}\ \sqrt{C^2/\alpha_1^2 - 1}}{(2 - C^2/\beta_1^2)^2} \quad \ldots\ldots\ldots\ldots\ldots \quad (2.34a)$$

and

ran

wre

Equa

disp

f; w

that

a li

rati

exis

indi

tion

and

$$\tan\left(\frac{2\pi f_r h}{\alpha_1}\cos\theta\right) = -\frac{\sqrt{C^2/\alpha_1^2 - 1}}{\sqrt{1 - C^2/\alpha_2^2}} \quad \ldots\ldots\ldots\ldots\ldots \quad (2.34b)$$

where θ = incident angle of P wave in the surface layer.

Equation (2.34b) involves only f_r which is related to the dispersion pattern, whereas equation (2.34a) involves only f_i which controls the attenuation of the amplitude. Note that equation (2.34b) is exactly the normal mode equation in a liquid layer overlying a liquid half-space with a density ratio of unity. If the above analysis is correct, the existence of the pipe organ type modes on land will be an indication of the existence of water-table. More observational evidence is needed to verify it.

Chapter III
Spectral Analysis and Data Interpretation

Spectrum, dispersion, arrival time, time duration, amplitude, particle motion, cross-spread velocity, etc. are useful in identifying a signal and in deducing model parameters. A body wave usually has a definite arriving time and short signal length. In contrast, the arrival of a normal or a leaking mode is not as sharp as the arrival of a body wave and the time duration is always much longer. Therefore, in studying a body wave, the determination of the arrival time is important. On the other hand, in studying the normal or leaking mode, the derivation of the dispersion pattern is stressed. In this chapter, we will discuss methods of identifying signals or deriving group velocities, and present the properties of signals identified on our records.

A. Methods Used to Identify Signals or Derive Group Velocities

Various methods used in identifying signals or deriving group velocities are introduced below. The discrete Fourier transform (DFT) and discrete inverse transform which will be used in these methods are given as follows: (Gold and Rader, 1969)

$$F(m\Omega) = \sum_{n=0}^{N-1} f(n\Delta)\ \exp(-jmn\,\Delta\Omega) \qquad (3.1)$$

$$f(n\Delta) = \frac{1}{N}\sum_{m=0}^{N-1} F(m\Omega)\ \exp(jmn\,\Delta\Omega) \qquad (3.2)$$

where

$F(m\Omega)$ = discrete form of the Fourier transform
$f(n\Delta)$ = discrete form of the time function
N = total data points in the time window
Δ = sampling time interval
$j = \sqrt{-1}$
$= 2\pi/(N\Delta)$
$m = 0, 1, 2, \ldots, N-1$
$n \quad 0, 1, 2, \ldots, N-1.$

The same formulas will also be used in other chapters. Note that for a particular data points N and a particular sampling interval Δ , there is a particular set of frequencies corresponding to them. For example, N=400 and Δ=0.005 sec., the corresponding frequencies are $m\Omega/(2\pi)$ = o, 1/2, 1, 3/2,..,399/2.

1. Moving Window Spectral Analysis Method

A typical feature of a surface wave record is that many modes are superimposed on each other and the spectral properties of each mode varies with time at different rates. If one is able to determine the exact amplitude and phase spectra at each time instance the separation of modes will easily be made and the group velocity dispersion curve of each mode will readily be found. Unfortunately, this particular method is not a feasible task. The uncertainty principle in spectral analysis states that the product of the spectral bandwidth (a measure of the bandwidth of the signal) and the time duration of a signal cannot be less than a certain minimum value (Hsu, 1970, p. 229). That is, the shorter the time window the poorer the frequency resolution, and the converse is also true. A compromise must be made between the length of the time window and the frequency resolution.

a. Parameters Involved in Use of the Method

The parameters considered in designing this method are: 1) the minimum time window for which the discrete Fourier transform is applicable; 2) the time window that is required to resolve the spectrum of our available records to the extent that each signal of interest is visually distinguishable; 3) the weighting function; and 4) the increment of window shift along the time axis.

To determine the minimum time window required, such that the spectrum, corresponding to a particular frequency $m\Omega/2\pi$ is derivable by using the discrete Fourier transform, consider the Fourier transform of a time function $f(n\Delta)$. Let us rewrite equation (3.1) as follows:

$$F(m\Omega) = \sum_{n=0}^{N-1} f(n\Delta) \exp\left(-j\frac{2\pi n}{N/m}\right) = \sum_{n=0}^{N/m-1} f(n\Delta) \exp\left(-j\frac{2\pi n}{N/m}\right) + \sum_{n=N/m}^{2(N/m)-1} f(n\Delta) \exp\left(-j\frac{2\pi n}{N/m}\right) + \ldots + \sum_{n=(m-1)(N/m)}^{m(N/m)-1} f(n\Delta) \exp\left(-j\frac{2\pi n}{N/m}\right) \ldots (3.3)$$

Note that the exponential term $\exp\left(-j\frac{2\pi n}{N/m}\right)$ is periodic. For some $i = 1, 2, \ldots, m$, an arbitrary summation in equation (3.3) can be written as:

$$\sum_{n=(i-1)(N/m)}^{i(N/m)-1} f(n\Delta) \exp\left(-j\frac{2\pi n}{N/m}\right) = \sum_{l=0}^{N/m-1} f[(1+(i-1)(N/m))\Delta] \cdot \exp\left[-j\frac{2\pi}{N/m}(1+(i-1)(N/m))\right]$$

$$= \sum_{l=0}^{N/m-1} f[(1+(i-1)(N/m))\Delta] \cdot \exp\left[-j\left(\frac{2\pi l}{N/m} + 2\pi(i-1)\right)\right] \ldots (3.4)$$

$$= \sum_{l=0}^{N/m-1} f[(1+(i-1)(N/m))\Delta] \cdot \exp\left(-j\frac{2\pi l}{N/m}\right)$$

because i is an integer. Define

$$fi(l\Delta) = f\,[(l+(i-1)\ (N/m))\Delta\,].$$

The time origin of $fi(l\Delta)$ differs from the time origin of $f[(l+(i-1)\ (N/m))\Delta]$ by $(i-1)\ (N/m)\Delta$, i.e., $fi\ (l\Delta)$ is a time-shifted function of $f(l\Delta)$. Also define $F_i(\Omega')$ to be the Fourier transform of $fi(l\Delta)$ for the data points $n=(i-1)(N/m)$ to $n=i(N/m)-1$ assuming that N/m=integer. We can write

$$\begin{aligned} Fi\ (\ \Omega\ ) &= \sum_{l=0}^{N/m-1} fi\ (l\Delta)\ \exp(-j\,\tfrac{2\pi l}{N/m}) \\ &= \sum_{l=0}^{N/m-1} fi\ (l\Delta)\ \exp(-jml\Delta\,\tfrac{2\pi}{N\Delta}) \qquad \ldots\ (3.5) \\ &= \sum_{l=0}^{N/m-1} fi\ (l\Delta)\ \exp(-jml\Delta\,\Omega\ ). \end{aligned}$$

It is concluded that Ω' is equal $m\,\Omega$. Therefore both Fourier transforms, $F(m\Omega)$ and $Fi(m\Omega)$, are defined for the same frequency $\frac{m\Omega}{2\pi} = \frac{m}{N\Delta}$, except that $F(m\Omega)$ is defined for the data points from n=o to n=N-1 and $Fi(m\Omega)$ is defined for the data points from $n=(i-1)(N/m)$ to $n=i(N/m)-1$ only. Note that the number of data points in $Fi(m\Omega)$ is N/m which corresponds to a time interval of $(N/m)\,\Delta$.

This time interval is exact the period of the frequency $m/(N\Delta)$ defined by both $Fi(m\Omega)$ and $F(m\Omega)$. Thus $Fi(m\Delta)$ can be termed One-period Fourier transform. Equation (3.3) can therefore be written:

$$F(m\Omega) = F_1(m\Omega) + F_2(m\Omega) + \ldots + Fm(m\Omega), \quad \ldots\ldots\ldots \quad (3.6)$$

namely, a m-period Fourier transform is a sum of m one-period Fourier transforms. Note that for $N/m \neq$ integer, equation (3.6) is not valid. However, from the practical point of view, it is possible to approximate it. For example, N=100, m=3, and $\Delta=1$, then

$$\Omega = 2\pi/100$$

and

$$F(m\Omega) = F(3\tfrac{2\pi}{100}) \cong \sum_{n=0}^{\frac{100}{3}-1} f(n)\ \exp(-3j\tfrac{2n\pi}{100}) + \sum_{n=\frac{100}{3}}^{\frac{200}{3}-1} f(n)\ \exp(-3j\tfrac{2n\pi}{100})$$

$$+ \sum_{n=\frac{200}{3}}^{100-1} f(n)\ \exp(-3j\tfrac{2n\pi}{100}) \cong [\sum_{n=0}^{32} f(n)\ \exp(-3j\tfrac{2n\pi}{100}) + 1/3f(33)\exp(-3j\tfrac{66\pi}{100})]$$

$$+[2/3f(33)\exp(-3j\tfrac{66\pi}{100}) + \sum_{n=34}^{65} f(n)\exp(-3j\tfrac{2n\pi}{100}) + 2/3f(66)\exp(-3j\tfrac{132\pi}{100})]$$

$$+[1/3f(66)\exp(-3j\tfrac{132\pi}{100}) + \sum_{n=67}^{99} f(n)\exp(-3j\tfrac{2n\pi}{100})]$$

$$\cong F1(3\tfrac{2\pi}{100}) + F2(3\tfrac{2\pi}{100}) + F3(3\tfrac{2\pi}{100}),$$

where F_1, F_2, and F_3 are the sums in the brackets [ ]. This approximation was tested on an exponential function. The maximum phase error observed was ± 0.003 radians, or ±0.05%. This is negligible in practice. The percentage amplitude error corresponding to this phase error can be shown to be [1-Cos(0.0005α)]X100 , where α is the phase angle. It is a very small amount.

The one-period Fourier transform described above is a DFT that is defined for the shortest time window, but it does not guarantee a satisfactory frequency resolution. It has been verified experimentally in this study that the five-period Fourier transform is a satisfactory one for our particular data.

The programming method is as follows: Firstly, N data points are divided into groups in subsequent order. For a particular frequency m/(NΔ), the number of points in each group is N/m, which corresponds to a time duration of N Δ /m, i.e., one period long. For example, N=400 and Δ=0.005 seconds, the number of points in each group are 400/m= ∞ , 400, 200, 133 1/3, ..., and 2 for m=0, 1, 2, ..., 200 (the maximum possible number in the first group is equal the maximum number of the available data points, i.e., 400). The corresponding periods are (400x0.005)/m=2/m= ∞ , 2, 1, 2/3, ..., and 2/200, and the corresponding frequencies are m/2=0, 1/2, 1, 1 1/2, ..., and 100. Secondly, the one-period complex Fourier transform is performed on each group of data points. Note that if the number of points in a group is not an integer, the approximation method mentioned

previously must be used. A five-period Fourier transform is then obtained by summing five one-period complex transforms to represent the complex spectrum of the central period of the five. To find the complex spectrum of the next time section, the five-period Fourier transform is shifted one period to the right (i.e., direction of increasing time).

The well known weighting functions such as Bartlett (triangular), Tukey (hanning), Hamming, Parzen, etc. are not easily programmed in the above process. A convenient method is to weight the five one-period transforms by 1/9, 2/9, 3/9, 2/9, 1/9, respectively and then sum them up to form the five-period transform. This kind of weighting is a rough version of the triangular weighting.

b. A Special Method for Improving Time Resolution

Since the shifting of the time window is in increments of one period, a further improvement in time resolution is desirable. The concept of Page's (1952) instantaneous power spectrum was used to accomplish this goal. The intuitive meaning of the so-called "instantaneous power spectrum" is the contribution of a single data point to the power spectrum of a time function which extends from minus infinity to a certain prescribed time. In application, it is assumed that the beginning time of a one-period time section, defined previously, is the time of appearance of a one-sided, (i.e., zero displacement before time of arrival) band-limited signal and the complex spectrum defined for the same time section is contributed mainly by this signal.

The following is the definition of Page's (1952) instantaneous power spectrum:

Parseval's theorem for the energy of a continuous signal may be written as:

$$\int_{-\infty}^{\infty} g^2(t)\,dt = \int_{-\infty}^{\infty} |F(f)|^2\,df \qquad (3.7)$$

where g (t) is the time function,

F(f) is the frequency function,

t = time,

f = frequency,

| | denotes the absolute value.

Let $\rho(t,f)$ denote the instantaneous power of a particular frequency f and at certain time t. The energy expanded from time minus infinity up to time t is

$$\int_{-\infty}^{t} g^2(\tau)\,d\tau = \int_{-\infty}^{\infty} df \int_{-\infty}^{t} \rho(\tau, f)\,d\tau \qquad (3.8)$$

by using the definition of $\rho(\tau,f)$ and the identity, equation (3.7). The instantaneous power of all frequency at time t is found to be

$$g^2(t) = \int_{-\infty}^{\infty} \rho(t,f)\,df \qquad (3.9)$$

by differentiating equation (3.8). Define a causal time function

$$g_t(\tau) = \begin{cases} g(\tau) & 0 < \tau \leq t \\ 0 & \text{otherwise} \end{cases} \qquad (3.10)$$

The Fourier transform of $g_t(\tau)$ is

$$Ft(f) = \int_{-\infty}^{\infty} g_t(\tau)\ \exp(-jw\tau)\ d\tau = \int_{o}^{t} g(\tau)\exp(-jw\tau)d\tau \quad (3.11)$$

The total energy of $g_t(\tau)$ is

$$\int_{-\infty}^{\infty} g_t^2(\tau)d\tau = \int_{o}^{t} g^2(\tau)d\tau = \int_{o}^{t} d\tau \int_{-\infty}^{\infty} \rho(\tau,f)df \quad (3.12)$$

by using equation (3.9). It can also be written as

$$\int_{-\infty}^{\infty} g_t^2(\tau)d\tau = \int_{-\infty}^{\infty} |Ft(f)|^2\ df \quad (3.13)$$

by using Parseval's theorem. By equating equations (3.12) and (3.13) we get

$$\int_{-\infty}^{\infty} df \int_{o}^{t} \rho(\tau,f)\ d\tau = \int_{-\infty}^{\infty} |Ft(f)|^2\ df \quad (3.14)$$

From equation (3.14), one can write

$$\int_{o}^{t} \rho(\tau,f)\ d\tau = |F_t(f)|^2 \quad (3.15)$$

Differentiating equation (3.15), obtain

$$\rho(t,f) = 2f(t)\,|Ft(f)|\ \ Re\ [\exp(jwt)\ \exp(j\alpha t,f)]$$

$$= 2f(t)\ |Ft(f)|\ Cos\ (wt + \alpha t,f) \quad (3.16)$$

where $\alpha_{t,f}$ denotes the phase of Ft(f).

Equation (3.16) was used in computing the instantaneous power spectrum. Note that $\rho(t,f)$ may be negative, but the cumulative energy $\int_0^t \rho(\tau,f)\,d\tau$ is always positive at all frequencies by equation (3.15). A negative $\rho(t,f)$ indicates a temporary readjustment to the total energy. Although the positive $\rho(t,f)$ does not necessarily indicate the presence of a particular frequency at time t, a successive building up of the positive power is no doubt a good indication. With this in mind, the positive densities are reduced by an amount proportional to the ratio of the negative sum to the positive sum and the negative densities are reduced by an amount proportional to the ratio of the negative sum to the positive sum and the negative densities are arbitrarily assigned zero values because they are not associated with the major signals in the time window. The isolated positive densities are again eliminated because they are apparently not associated with long duration normal or leaking modes.

c. Uses of Moving Window Spectral Analysis Method

The moving window spectral analysis method may be used for two purposes. One is for separating superimposed modes and for revealing time-varying spectra. Another is for deriving group velocity dispersion curves.

Figure 3 shows the second and third "pipe organ" modes, on a portion of the 2nd [illegible] trace of record No. 43, being separated by this method. This figure also indicates that the first mode (frequency about 10 HT[illegible]) does not appear right after the refracted α_2 arrival. The observed points in

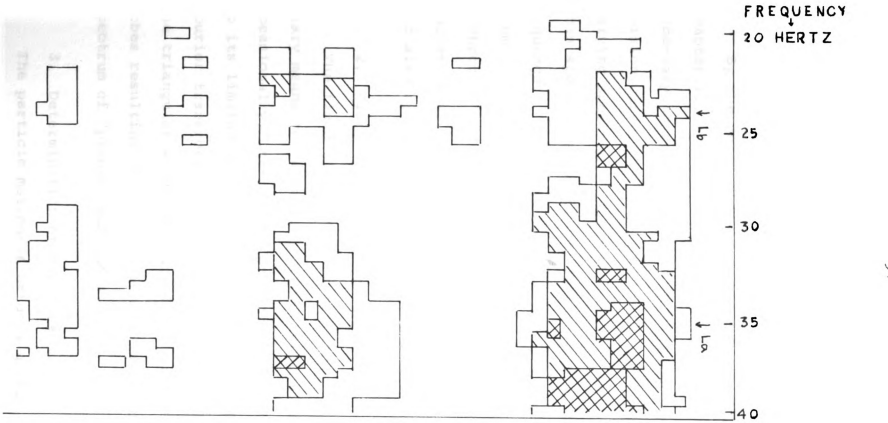

FIGURE 3. TIME-VARYING SPECTRA OF MULTIPLE REFLECTIONS
(RECORD NO. 43, SECOND Z TRACE)

Figures 4 and 5 are the peaks of the time-varying spectra of the subsequent time sections of the same record. Two superimposed modes are identified in Figure 5. The events, La, Lb, Lc, etc. are defined in Table 3, p. 52.

By the definition of group velocity, introduced in Chapter II, a curve obtained by connecting the peaks of a time-varying spectrum is the observed group velocity dispersion curve of a particular mode. Figure 6 shows the time-varying spectrum of M_{11} mode. Due to the limited space, this spectrum is drawn separately on four pages in original sequence. The circles indicated are the peaks of the spectrum. The group velocity dispersion curve is obtained by connecting these circles. Figure 7 shows the group velocity curves of M_{11} mode found on several records by this method and also by hand picking.

2. Fixed Window Fourier Transform

The fixed window Fourier transform is used as an auxiliary means to the moving window spectral analysis method. Occasionally, the latter does not reveal clear spectrum due to its limited length of time window, the fixed window Fourier transform must be applied using a longer time window. The triangular weighting function is used to reduce the side lobes resulting from truncation. Figures 8 and 9 are the spectrum of "pipe organ" modes.

3. Determination of Particle Motion

The particle motion is often a useful means in identi-

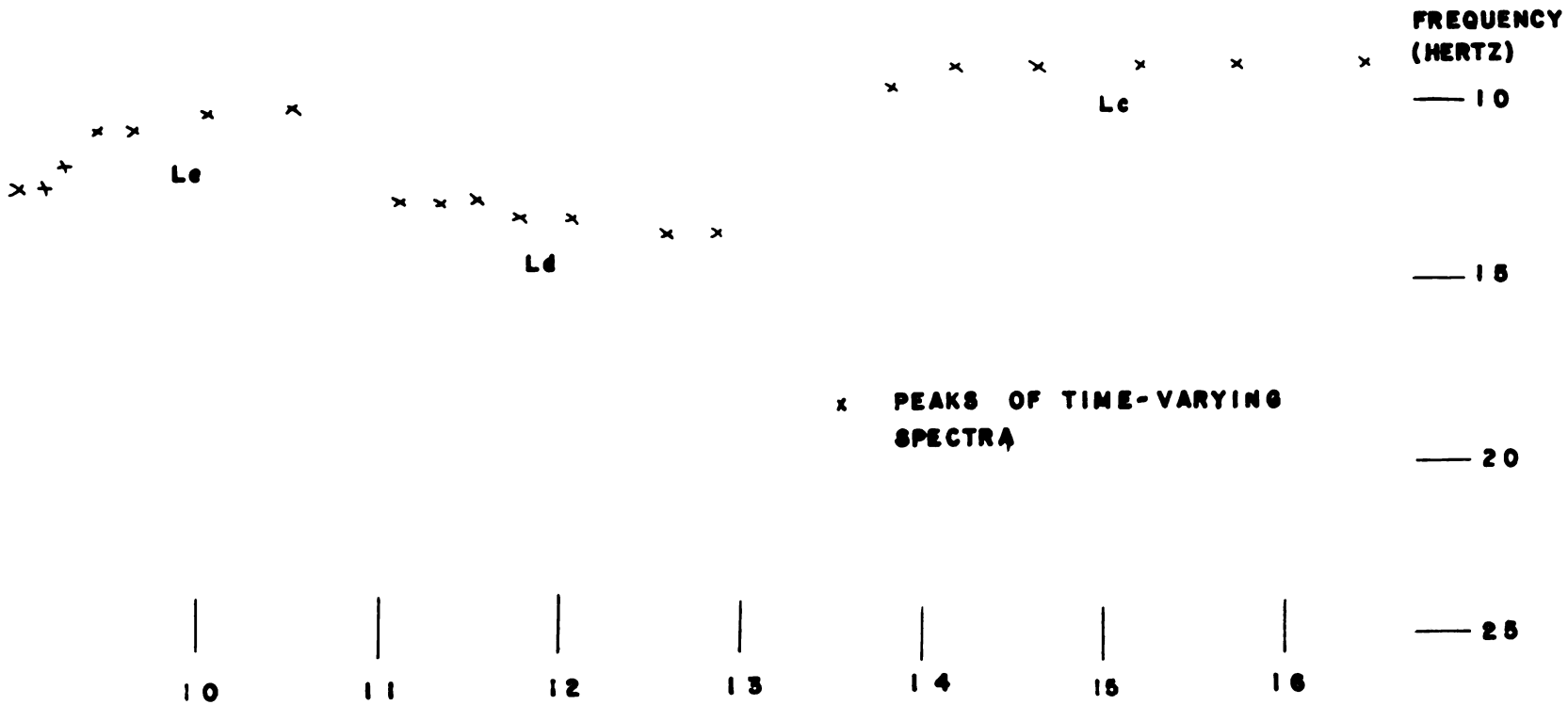

FIGURE 4. EVENTS WITH DISTINCT TIME-VARYING SPECTRUM (RECORD NO. 43, SECOND Z TRACE)

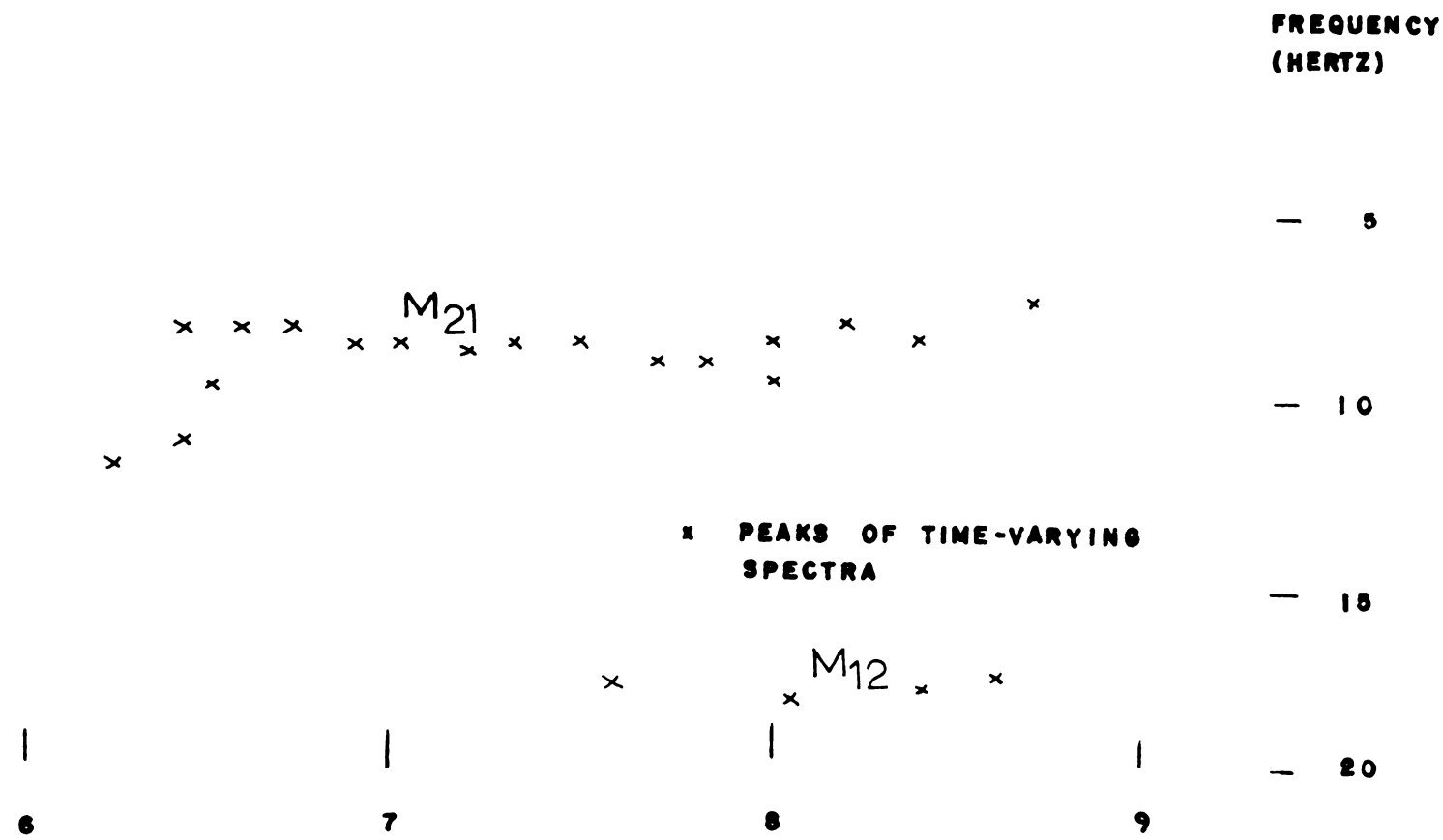

FIGURE 5. EVENTS WITH DISTINCT TIME-VARYING SPECTRUM (RECORD NO. 43, SECOND Z TRACE)

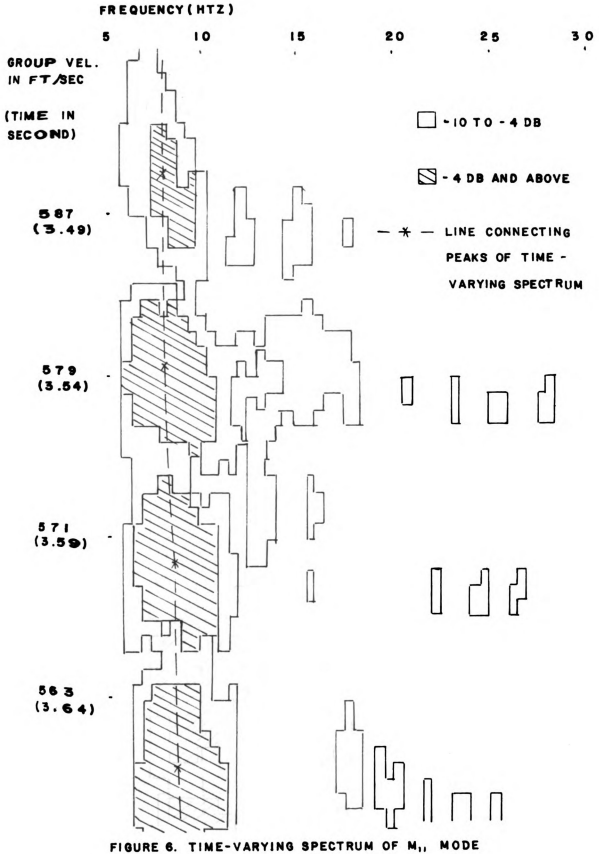

FIGURE 6. TIME-VARYING SPECTRUM OF M_{11} MODE
(RECORD NO. 43, SECOND Z TRACE)

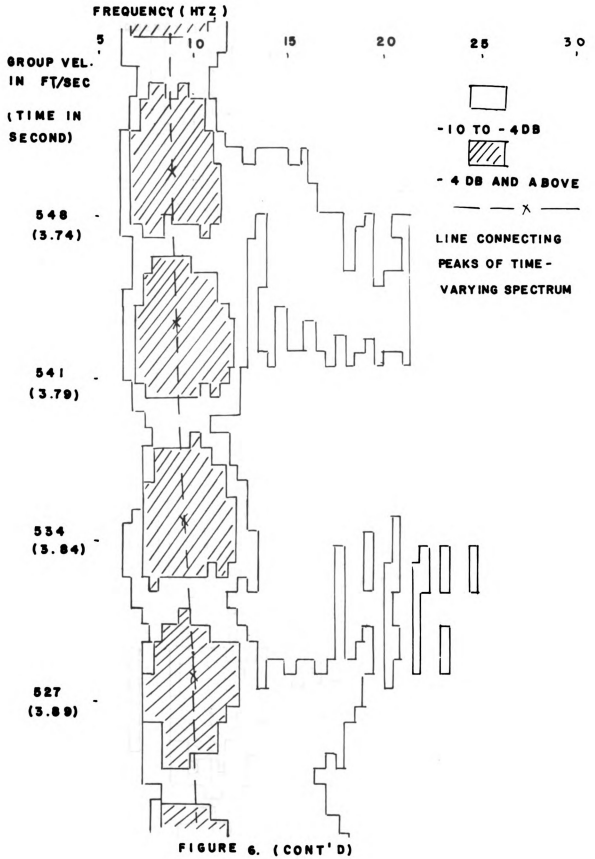

FIGURE 6. (CONT'D)

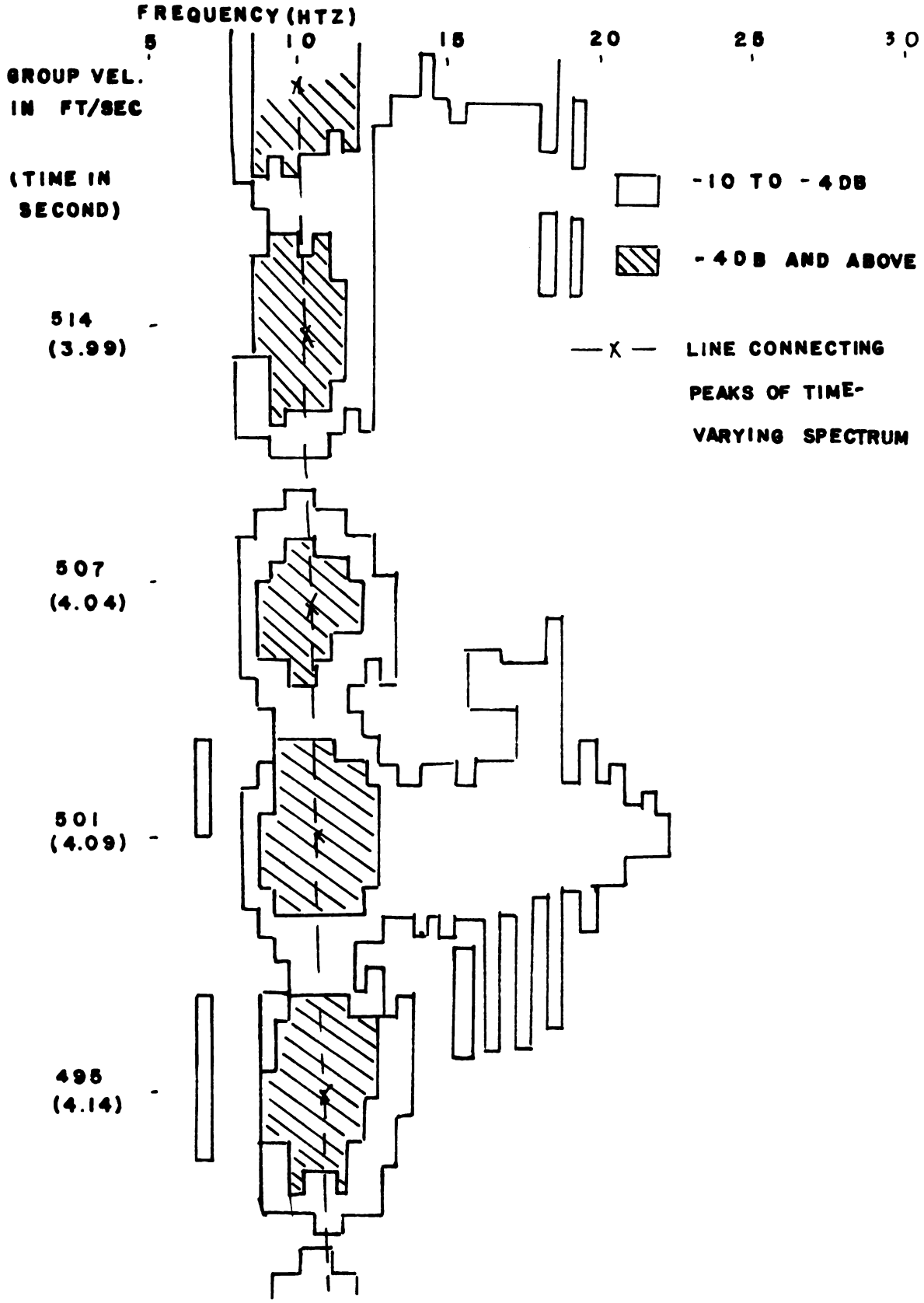

FIGURE 6. (CONT'D)

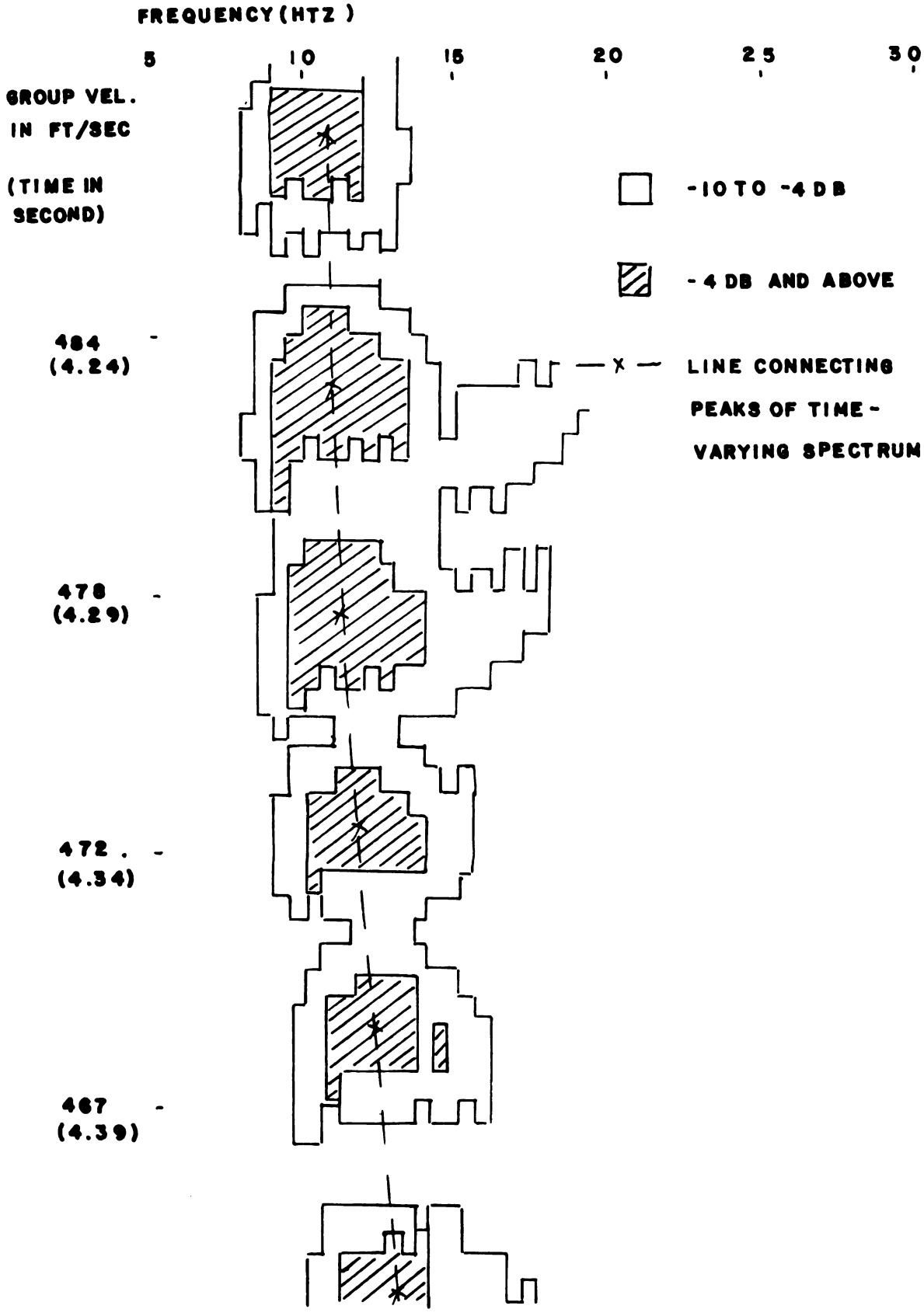

FIGURE 6. (CONT'D)

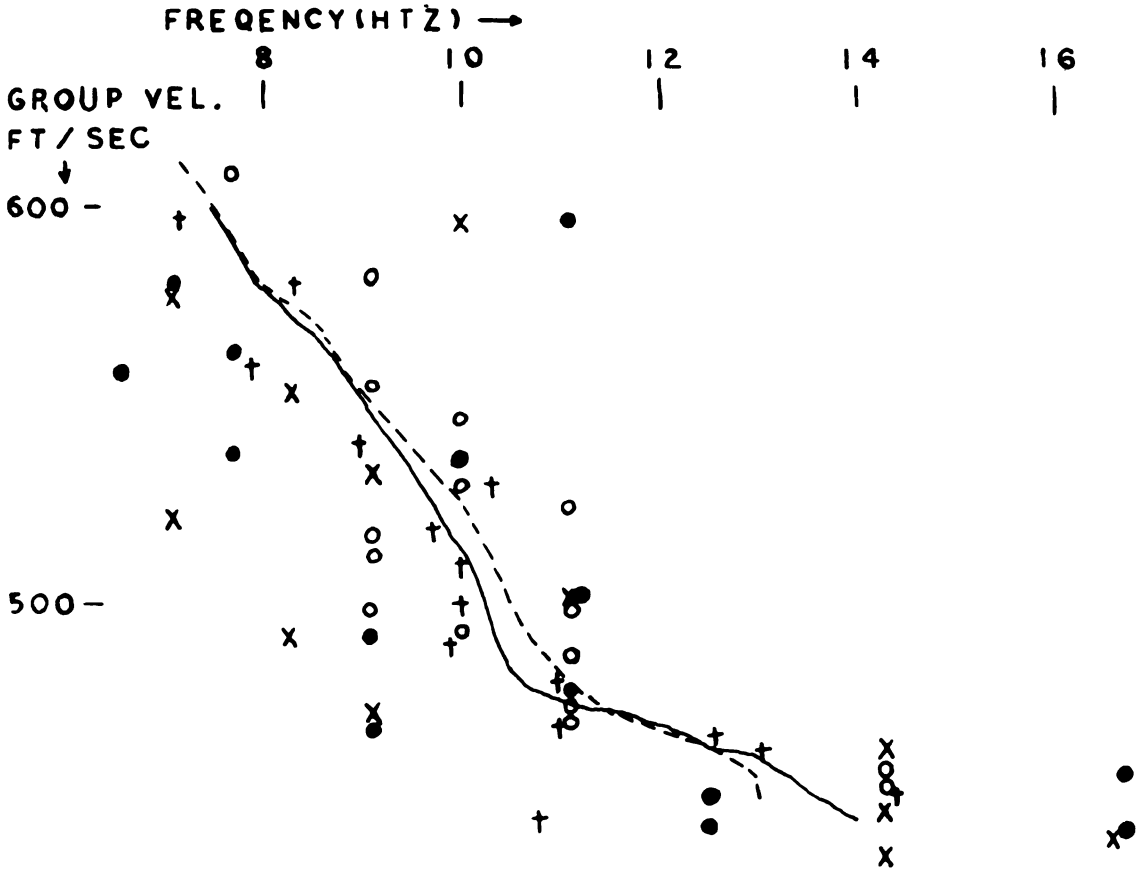

MOVING WINDOW SPECTRAL ANALYSIS METHOD

SYMBOL	RECORD NO.	COMPONENT	TRACE NO.
———	43	Z	2
– – –	43	Z	6

DIRECT MEASUREMENT OF PERIODS AND ARRIVAL TIMES

SYMBOL	RECORD NO.	COMPONENT	TRACE NO.
X	33	Z	2
●	33	Z	3
o	43	Z	2
†	43	Z	8

FIGURE 7. OBSERVATIONAL GROUP VELOCITIES OF M_{11} MODE

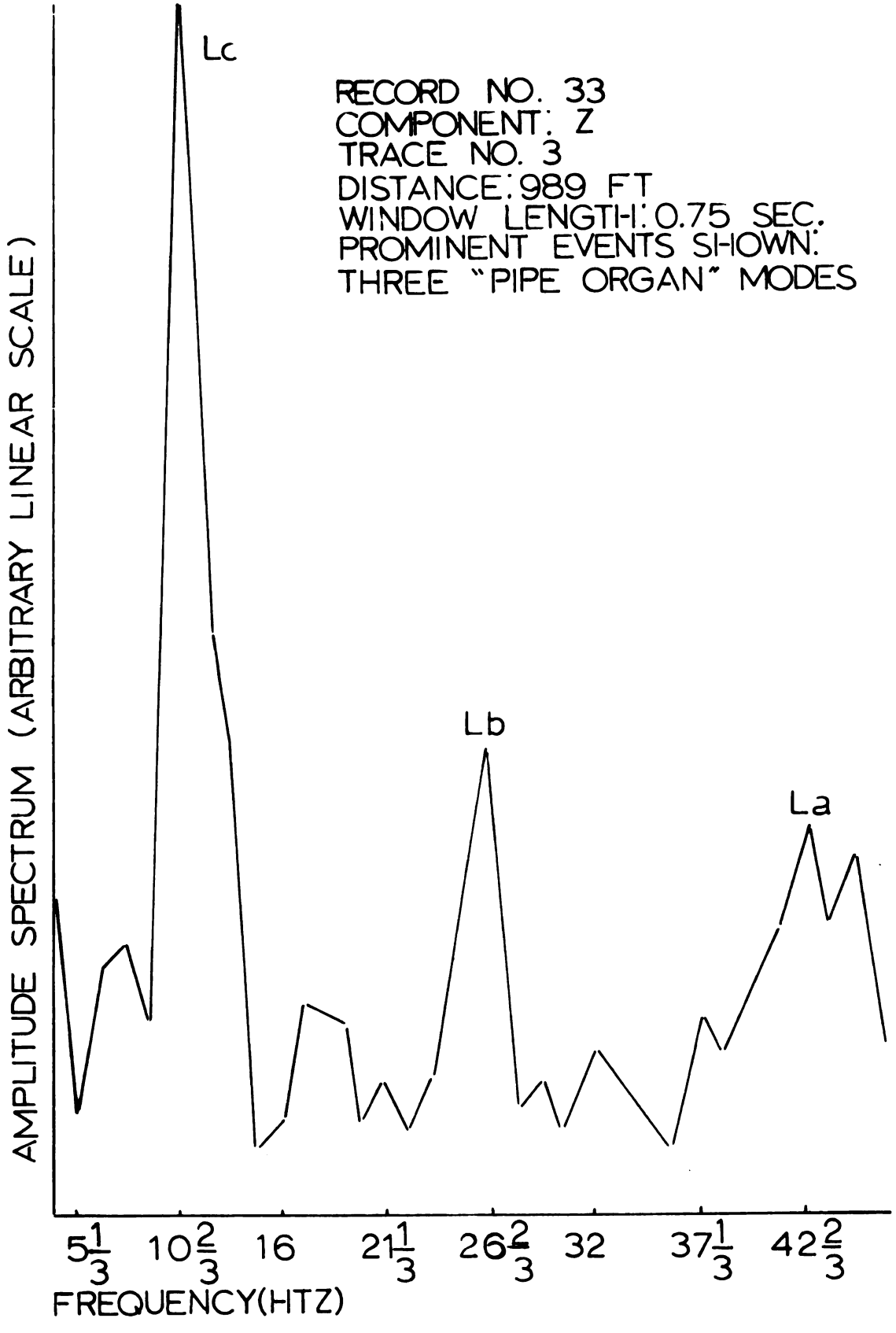

FIGURE 8. AMPLITUDE SPECTRUM (FIXED WINDOW)

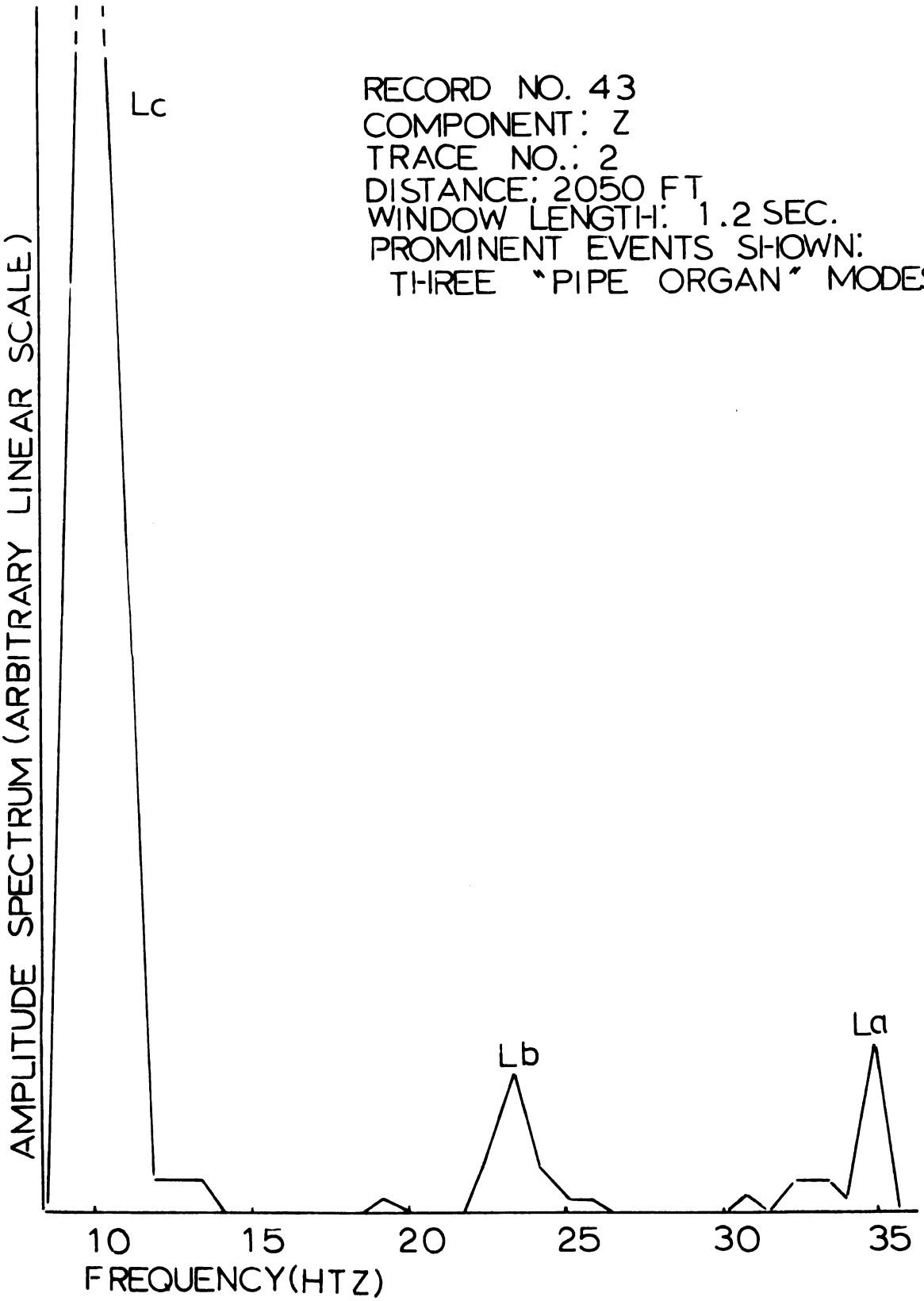

FIGURE 9. AMPLITUDE SPECTRUM(FIXED WINDOW)

fying a signal. The determination may be accomplished by superimposing the X trace on the Z trace and inspecting the phase lags between two traces. This method is illustrated in Figure 10. The particle motion is one of the properties of events identified in Table 3.

B. Interpretation of Data

The refraction records that have been studied are listed in Table 2. The spacing between any two adjacent geophones, charge size, depth of shot hole, and the distance between shot and the spread are indicated. These records were recorded without automatic gain control (AGC), suppression, and filter setting. Because no part of the spectral band is negligible under theoretical consideration, any distortion, caused by the artificial means, should be avoided. The high frequency noises such as those due to instrument, wind motion, etc. can be filtered out after a visual inspection of the spectrum is made.

The data used for the study were digitized from the paper records. The errors introduced by the digitizing process are not easy to evaluate. To test for errors in digitization a trace was digitized twice and the average was determined. There was no noticeable improvement in the result, thus we conclude that digitization errors were negligible. Most of the data used was thus digitized only once.

The characteristic seismic events having been identified on seismic records by methods described previously are

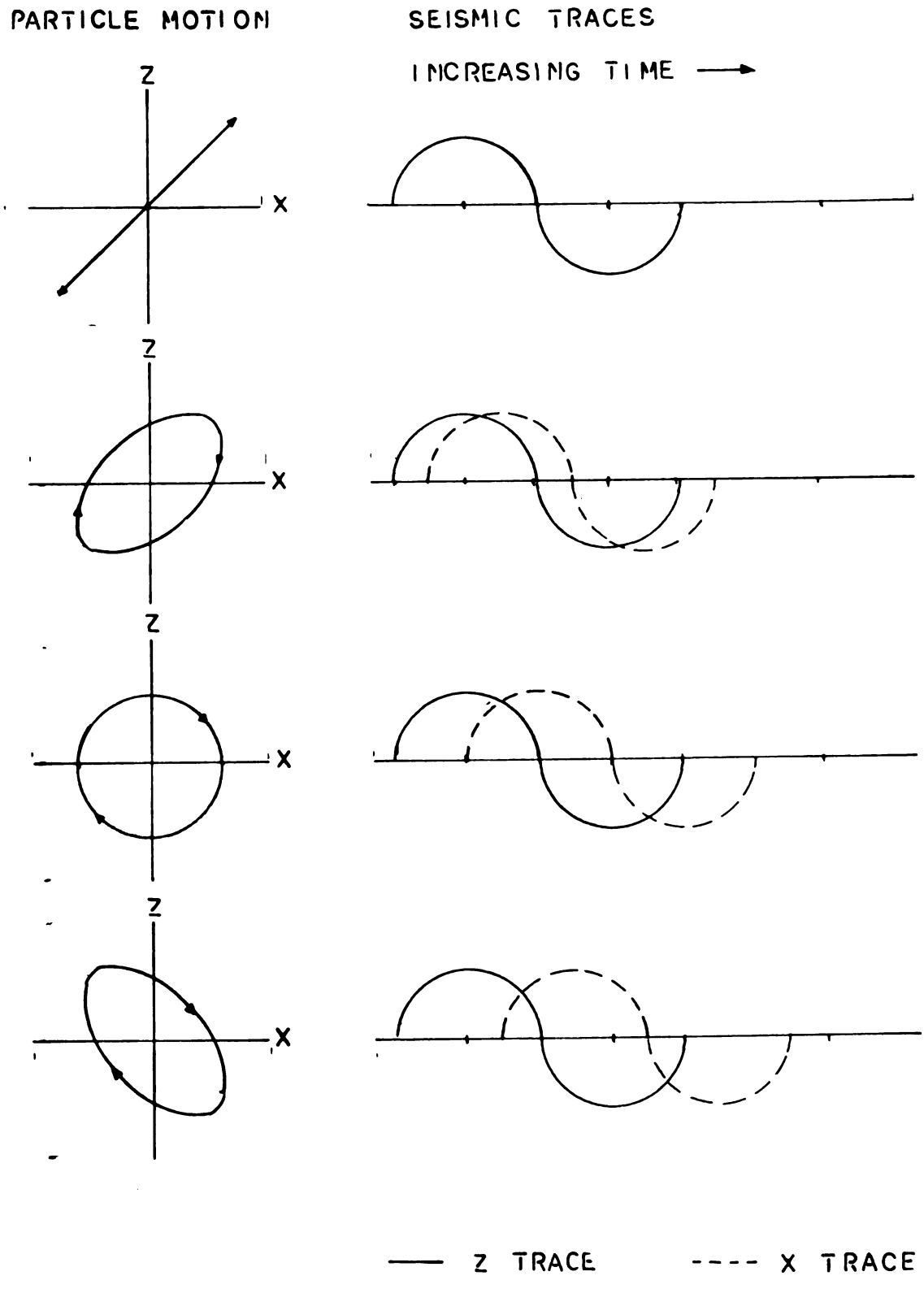

FIGURE 10. DETERMINATION OF PARTICLE MOTION

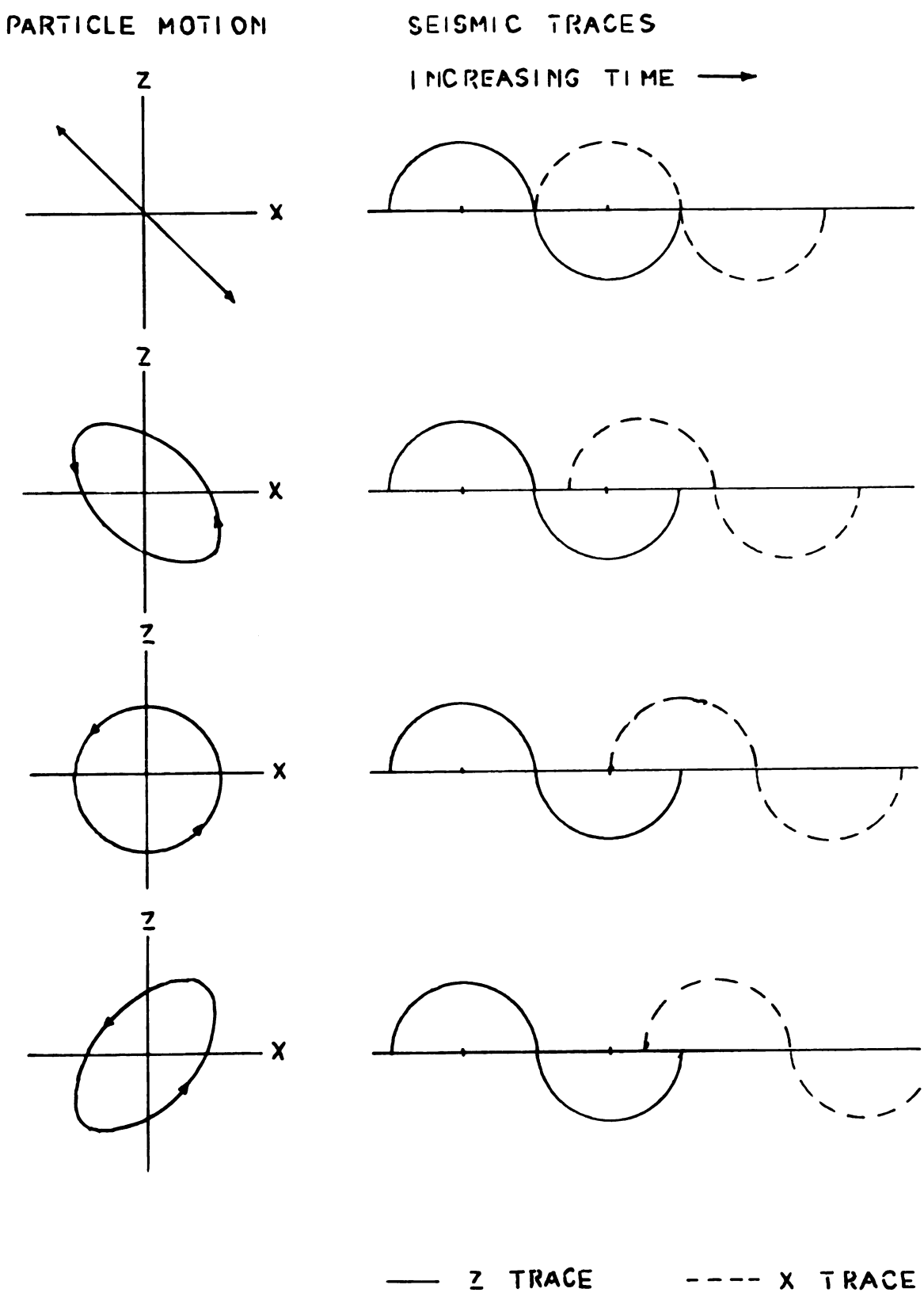

FIGURE 10. (CONT'D)

Table 2. List of Refraction Records

Record Number	Spacing (ft)	Charge (lb)	Hole Depth (ft)	Distance From End of Spread (ft)
10	25	2	5	725
11	25	2	5	725
33	10	16	10	969
34	10	4	10	600
42	50	8	10	2000
43*	50	8	10	2000

*Repeated version of record No. 42, except that No. 43 has lower gain setting than No. 42.

Table 3. List of Events

Event	Dispersion	Peak Freq. (cps)	Freq. Band (cps)	Gr. Vel. (ft/sec)	Cross Spread Vel.(ft/sec)	Particle Motion	Remark
α_3	----	----	20 & above	----	13461	?	Refracted P from bed rock
α_2	----	----	20 & above	----	5700	?	Refracted P from saturated layer
Lb	?	26.557 (at 969') 23.33 (at 2000')	---	4505 - 3228	----	?	2nd "pipe organ" Short duration
La	?	42.667 (at 969') 35.00 (at 2000')	---	4505 - 3228	----	?	3rd "pipe organ" Short duration
Lc	Normal	9.0 - 11.5	---	1900 - 1366	----	Retro-grade	1st "pipe organ"
Ld	Reverse	15.0 - 11.5	---	1330 - 1000	1750 (at 2000') 1100 (at 969') 1345 (at 725')	Pro-grade	Leaking mode coupled to direct P (?), High amplitude in X, Y, & Z components
Le	Normal	11.5 - 13.5	---	1000 - 900	----	Pro-grade	Continuation of Lc (?)
β_2	----	----	11 - 30	About 905	905	?	Refracted S, High ampl. in X component
M21	Normal	7.5 - 11.5	---	870 - 627	---	Prog. to Retrog.	Normal mode
M12	?	17.5 - ?	---	861 - 760	---	?	Normal mode
M11	Normal	4.0 - 13.0	---	628 - 445	---	Pro-grade	Normal mode

?Unable to determine

listed in Table 3 (events on Y component are not included).

La, Lb, ...Le are leaking modes arriving before the refracted shear wave β_2 . La, Lb, and Lc are actually multiple reflections of refracted P wave α_2 . We have discussed their spectral properties and the underlying theory in Chapter II. Ld is a peculiar event. It is dispersive and has a cross spread velocity similar to the P wave velocity in the surface layer, i.e., 1150 ft/sec. It may be interpreted that when the direct P wave couples to Lc, it results in a low frequency, high amplitude disturbance which has a cross spread velocity of the P wave in the layer and also exhibits the properties of a leaking mode. Le, being interpreted as the continuation of Lc, is solely based upon the similarity in spectral bands. That β_2 is being related with the refracted S, can be due to the following evidences: 1) high amplitudes appear in X component (at distances, 989' and 2050') indicating a disturbance with strong shear motion; 2) cross spread velocity and group velocity (more correctly, shot-receiver distance/arriving time) are both about 900 to 905 ft/sec, indicating a refracted event from the half-space; moreover, the S velocity in the half-space is found to be in this range by the inversion of observational phase velocities (discussed in Chapter V; 3) all normal modes appear after this event (the highest velocity of normal modes is S velocity in the half-space). The normal modes M_{21}, M_{12}, and M_{11} are identified on the basis of their time-varying spectra. The particle motion of

M_{21} and M_{11} are found to be consistant with the theoretical calculations made by Mooney and Bolt (1966) for the alluvium case.

There are many other events that are possible of identification on the records, for example, the one identified by Bennett (1973) to be due to P-S conversion. The study was limited to those events that are easily detectable by moving or fixed window spectral analysis, and those that have apparent relations to our single surface layer model. Further discussion concerning the events and their implications in the assumed model are found in Chapter VI.

Chapter IV
Methods of Computing Phase Velocities From Observational Data

Various methods of computing phase velocities using observational data are discussed in this chapter. The computed phase velocities will be inverted to yield model parameters. The details of the inversion is given in Chapter V.

A. Peak-and-trough Method

Having been mentioned in Chapter II, the phase velocity is the velocity with which the wave form propagates. On a seismic record, it is possible to correlate a particular wave form from one trace to another, provided that: 1) the distance between two stations is not excessive; 2) the noise level is not excessive; 3) no superimposed events are present. The phase velocity is computed by dividing the distance between two stations by the time shift of this wave form on two traces and the corresponding frequency is determined by measuring the period of this wave form (Officer, 1958). The phase velocities of M_{11} mode obtained by this method, is shown in Figure 11. This is the oldest and the simplist method of estimating phase velocities. It is observed on Figure 11 that the results are poor.

B. Fourier Transform Methods

The underlying theory is the same for all the methods that will be discussed in this section. Consider that a dispersive event observed at station A is $f_A(t)$, and the same

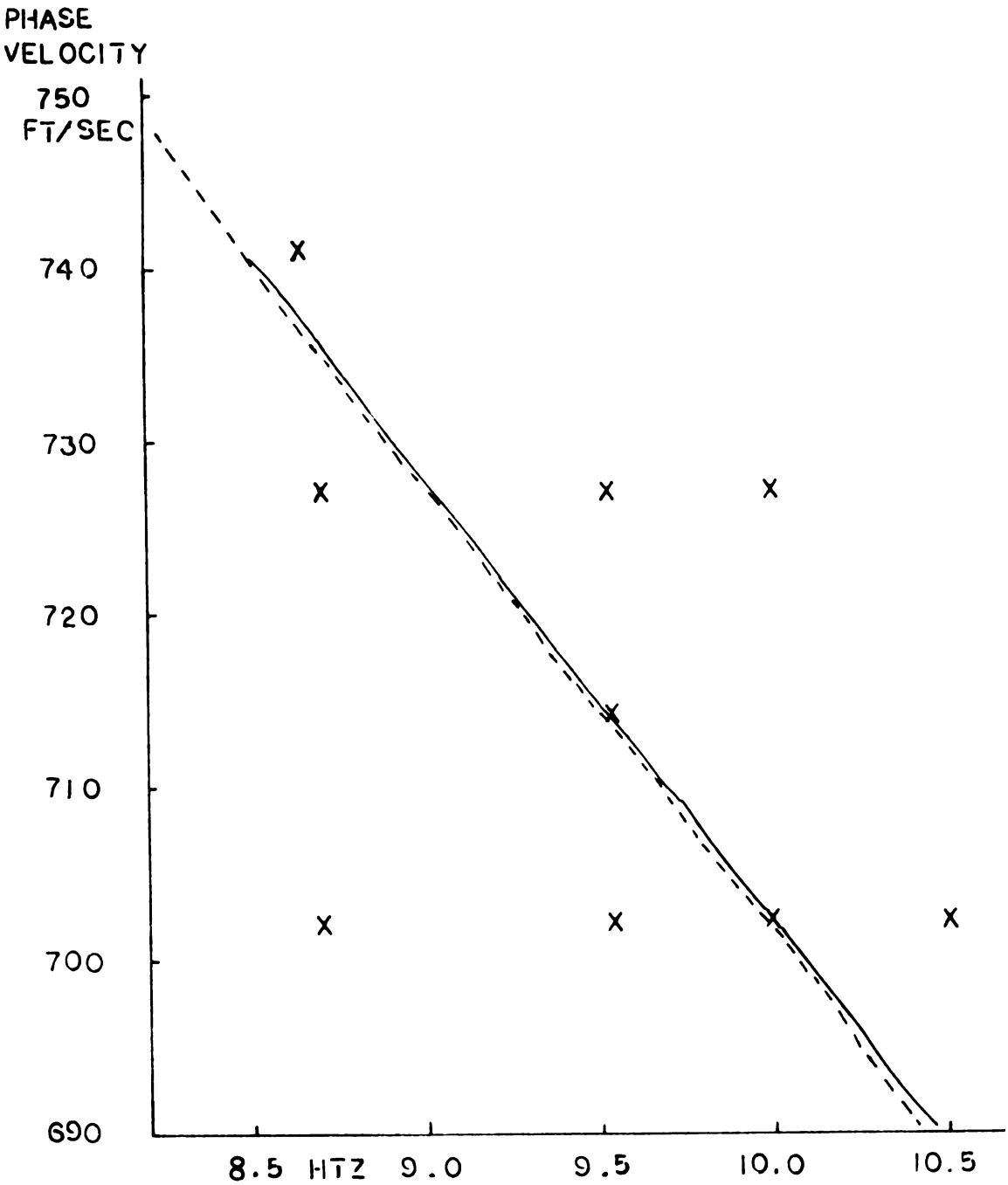

X PEAK-AND-TROUGH METHOD (2ND AND 6TH Z TRACES)

--- FOURIER SUM-AND-DIFFERENCE METHOD (2ND AND 6TH Z TRACES)

—— INTEGRATION OF THE OBSERVATIONAL GROUP VELOCITY DISPERSION CURVE (2ND Z TRACE)

FIGURE 11. PHASE VELOCITIES OF M_{11} MODE (RECORD NO. 43)

event observed at station B is $f_B(t)$. The Fourier transform of $f_A(t)$ and $f_B(t)$ are $F_A(w)$ and $F_B(w)$, respectively. The difference in amplitude spectra between $F_A(w)$ and $F_B(w)$ may be due to geometric spreading, and material dissipation, and the difference between phase spectra is due mainly to the difference between arriving times, i.e., dispersion. The phase velocity can be found by the formula given by Sato (1960):

$$\Delta\alpha \pm 2m\pi = w\ \Delta t = 2\pi f\ (r_B - r_A)/C(f)$$

or

$$C(f) = 2\pi f\ (r_B - r_A)/(\Delta\alpha \pm 2m\pi), \qquad (4.1)$$

where r_A and r_B are shot-receiver distances at station A and station B, respectively, $\Delta\alpha = \alpha_A - \alpha_B$ = phase difference, and m=0, 1, 2, 3, ---, Δt= time shift of the same wave form in two traces.

1. Fourier Phase Difference Method

This method finds phase difference by subtracting the phase spectrum of $F_B(w)$ from the phase spectrum of $F_A(w)$ directly, and then uses equation (4.1) to find phase velocity. It was applied to the data of this study, but the results obtained were very poor. The reason is probably due to the short time duration of signals and to rapid change of spectral properties.

2. Crosscorrelation Method

The crosscorrelation functions of two functions $f_A(t)$ and

$f_B(t)$ is defined as: (Hsu, 1967)

$$R_{AB}(\tau) = \int_{-\infty}^{\infty} f_A(t)\ f_B(t-\tau)\ dt \qquad \ldots\ldots\ldots\ldots\ldots\ldots \quad (4.2)$$

and

$$R_{BA}(\tau) = \int_{-\infty}^{\infty} f_B(t)\ f_A(t-\tau)\, dt$$

the Fourier transform of $R_{AB}(T)$ is

$$F_A(w) \cdot F_B(-w) = \left| F_A(w) \right| \cdot \left| F_B(w) \right| \exp(j\Delta\alpha)$$

and the Fourier transform of $R_{BA}(T)$ is

$$F_A(-w) \cdot F_B(w) = \left| F_A(w) \right| \cdot \left| F_B(w) \right| \exp(-j\Delta\alpha).$$

Theoretically, the crosscorrelation can be performed either in frequency or time domain. Landisman, et al.(1969) claims that the phase velocity dispersion curve obtained first by crosscorrelating two functions in the time domain and then taking the Fourier transform are smoother than those found by the Fourier phase difference method described previously.

This method was also used on the data of this study by means of computer program provided by Dr. R. S. Carmichael of the Department of Geology. The results did not seem to be much better than the results using the Fourier phase difference method.

3. Fourier Sum-and-difference Method

This method, instead of making use of the phase difference directly, calculates the amplitude spectrum of the sum

or difference of the two functions $f_A(t)$ and $f_B(t + \Delta t)$, where Δt = time shift with respect to the time origin of $f_A(t)$. The Fourier transform of these two time functions are $F_A(f)$ and $F_B(f)\ \exp(jw\Delta t)$, respectively. The phase velocity is found by

$$C = (r_B - r_A) / \Delta t \qquad (4.3)$$

and the corresponding frequency is the frequency that exhibits maximum or minimum amplitude spectrum, depending on the sum or the difference being used.

The details of this method can be found in Bloch and Hales (1968). A brief explanation of how this method works is given below for reference: Let

$$S(f) = F_B(f)\ \exp(jw\Delta t) + F_A(f),$$
$$D(f) = F_B(f)\ \exp(jw\Delta t) - F_A(f).$$

Assume the amplitude spectra of $F_B(f)$ and $F_A(f)$ are the same (in application, this can be accomplished by normalization), i.e., both equal some constant A. S(f) can also be written as:

$$S(f) = F_B(f)\ \exp(jw\Delta t) + F_A(f) = A[\exp(j\alpha_B)\cdot \exp(jw\Delta t) + \exp(j\alpha_A)] = A\ [(\cos(\alpha_B + w\Delta t) + \cos\alpha_A)^2 + (\sin(\alpha_B + w\Delta t) + \sin\alpha_B)^2]^{1/2} \exp\left[j \tan^{-1} \frac{\sin(\alpha_B + w\Delta t) + \sin\alpha_A}{\cos(\alpha_B + w\Delta t) + \cos\alpha_A}\right]$$

$$= A\ 2^{1/2}\ [1 + \cos(\alpha_B - \alpha_A + w\Delta t)]^{1/2} \cdot \exp\left[j \tan^{-1} \frac{\sin(\alpha_B + w\Delta t) + \sin\alpha_A}{\cos(\alpha_B + w\Delta t) + \cos\alpha_A}\right]. \qquad (4.4)$$

When the absolute value of S(f) is a maxima,

$$\text{Cos}\ (\alpha_B - \alpha_A + w\,\Delta t) = 1$$

or

$$\alpha_B - \alpha_A \pm 2m\pi = \Delta\alpha \pm 2m\pi = w\,\Delta t \qquad (4.5)$$

It is the same as equation (4.1). Similarly D(f) can be written as:

$$D(f) = A2^{1/2}\,[1-\text{Cos}(\alpha_B - \alpha_A + w\,\Delta t)]^{1/2}$$

$$\cdot\exp\left[j\,\tan^{-1}\frac{\sin(\alpha_B + w\Delta t) - \sin\alpha_A}{\cos(\alpha_B + w\Delta t) - \cos\alpha_A}\right].$$

When the absolute value of D(f) is a minimum, the same conclusion results.

In application, the ratio $|D(f)|\,/\,|S(f)|$ is used so that the minima is more pronounced. A display of this ratio vs. time shift Δt is automatically printed out by the computer. The phase velocity dispersion curve is determined by correlating the minimum points of amplitude spectra corresponding to different time shifts.

Care must be exercised in determining the dispersion curve because for any time shift, the corresponding spectral minima is repeating for each period along the time-shift (or phase velocity) axis. This can be easily explained by using equation (4.1):

$$C(f) = 2\pi f\,(r_B - r_A)/(\Delta\alpha \pm 2m\pi) = (r_B - r_A)/(\Delta t \pm m \cdot \text{period}).$$

For m=0,1,2, ---, there are infinite values of phase velocities. This ambiguity can be resolved by checking with the results obtained by the peak-and-trough method described previously.

There are some additional procedures which were used to improve the results and to reduce the computing time:

a. Shifting Phase Spectrum

The Fourier transform is a time consuming process. The method used here was designed to perform the time shifting in frequency domain without resorting to repeating the Fourier transform. It can be shown that the Fourier transform of $f_B(t + \Delta t)$ is $\exp(jw\Delta t)\, F_B(w)$. For a time limited function, the multiplication of $F_B(w)$ by $\exp(jw\Delta t)$ is equivalent to the shifting of the time function. It is schematically illustrated in Figure 12.

This method has two advantages. Firstly, one needs to perform Fourier transform only once for the two time functions, $f_A(t)$ and $f_B(t)$, respectively. The Fourier transforms of $f_B(t + \Delta t_0)$, $f_B(t + \Delta t_1)$, $f_B(t + \Delta t_2)$, ...etc. are replaced by multiplying $\exp(jw\Delta t_0)$, $\exp(jw\Delta t_1)$, $\exp(jw\Delta t_2)$, ... etc. to $F_B(w)$. The saving in computer time is considerable. Secondly, the shifting of the windowed time function will not introduce any additional noise as will the actual shifting in

Shifted Time Increments	Position of Samples in Time Domain
0	0 1 2 3 4 5 6 7
1	7 0 1 2 3 4 5 6
2	6 7 0 1 2 3 4 5
3	5 6 7 0 1 2 3 4
4	4 5 6 7 0 1 2 3
5	3 4 5 6 7 0 1 2

Figure 12. An Example of Shifting in Time Domain

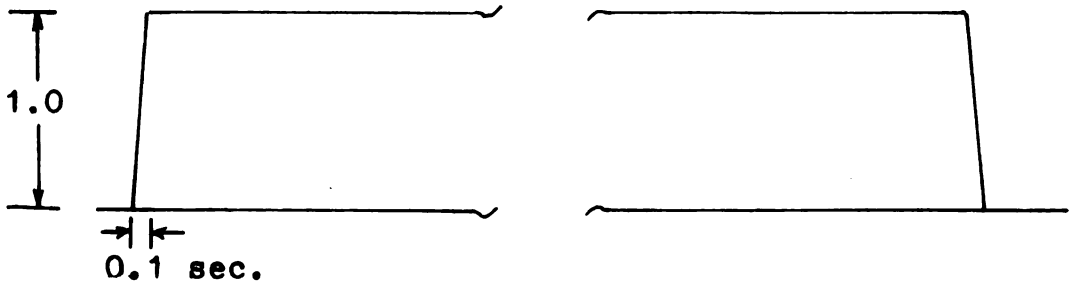

Figure 13. Trapezoidal Weighting Function

time. Since most of the signals on our records are short in duration, the introducing of a few noises will distort the spectrum substantially.

b. Normalization of Time Functions

This method of computing phase velocity is based upon the assumption that $F_A(w)$ and $F_B(w)$ both have the same amplitude spectrum. This is not true in practice. Two time functions, $f_A(t)$ and $f_B(t)$, were normalized with respect to the maximum amplitude in two functions.

c. Trapezoidal Weighting Function

A trapezoidal weighting function shown in Figure 13 is used to reduce the effects caused by trancations. Another reason for using this weighting function is to weight every sampling point in the window evenly, except for a few points near the truncations. This is done to avoid the possible distortion of the spectrum.

d. Time-varying Filter

All surface waves possess time-varying spectra. To filter out noises, a filter with time-varying pass-band is desirable. The principles in designing this filter are the same as those described in Landisman, et al.(1969). It was found that the phase velocity dispersion curves, determined by using the filtered data, were better than the unfiltered ones.

The method of applying this filter is given below:

Firstly, a fast Fourier transform is performed on the time function. Using the discrete Fourier spectrum obtained, one can compute the amplitudes and phases of the Fourier series which represents the time function. Secondly, by inspecting the time-varying spectra described in Chapter I, one is able to determine the pass-band of the signal at different time instances. Finally, the filtered signal is obtained by truncating each cosine function of the time series according to the shape of the time-varying spectrum and summing over all truncated cosine functions. The truncations of cosine functions are smoothed before summing by a half-cosine weighting function given below:

$$W(t) = \begin{cases} \cos\left(\frac{\pi t}{L}\right) & -L/2 < t \leq L/2 \\ 0 & \text{otherwise} \end{cases}$$

where L = length of the time window.

Having been mentioned in Chapter III, the evaluation of the one-period Fourier transforms was a first step in the computation of the time-varying spectra. This data was punched on cards by the computer during the computation. The summation of all the one-period transforms corresponding to a particular frequency is the Fourier transform of the time function. Again, a "cleaner" Fourier transform can be obtained by nulling those one-period Fourier transforms that fall into the rejecting bands. Figure 14 shows an

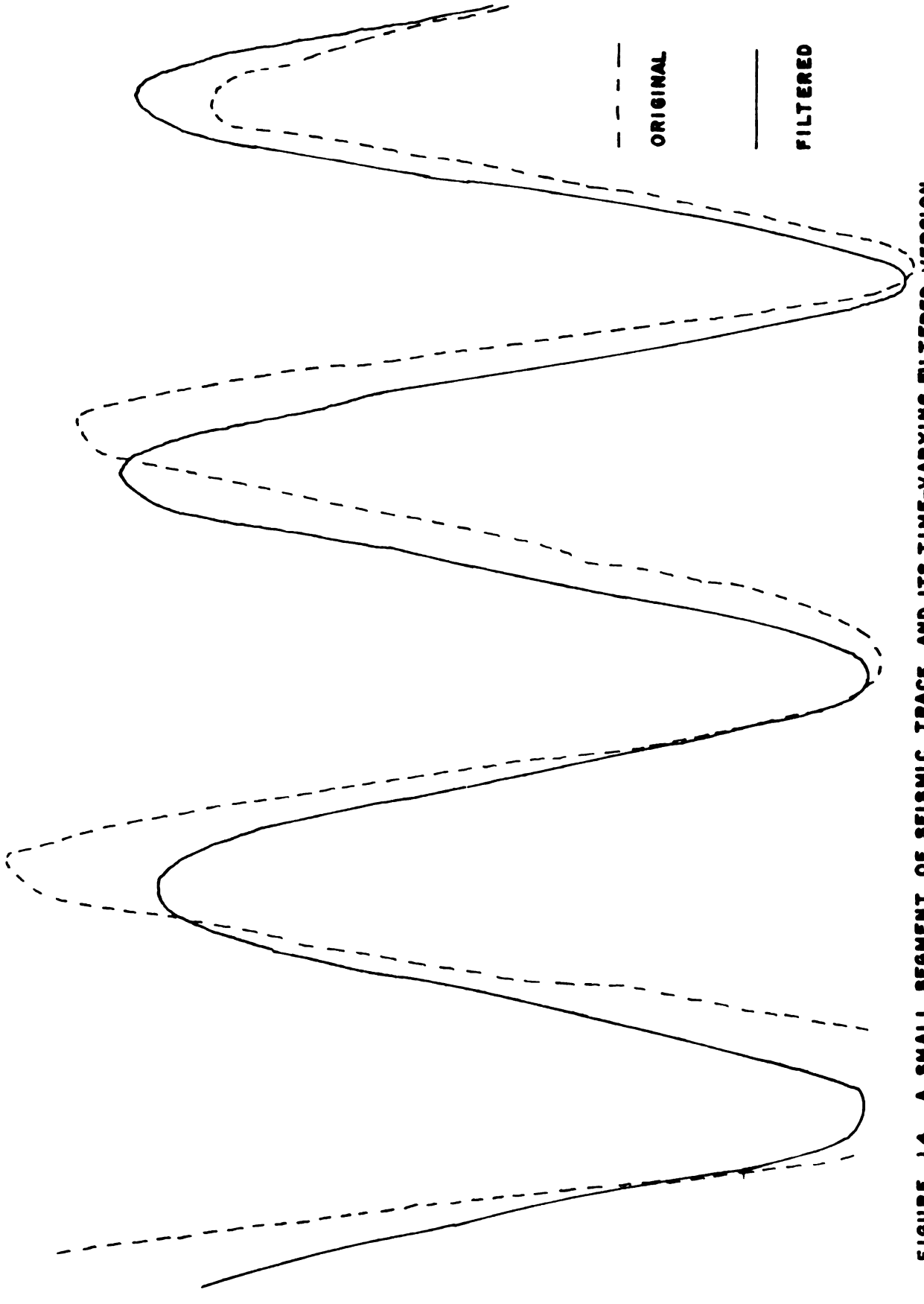

FIGURE 14. A SMALL SEGMENT OF SEISMIC TRACE AND ITS TIME-VARYING FILTERED VERSION

example of the filtered and the unfiltered M_{11} signal.

A phase velocity dispersion curve obtained by the Fourier sum-and-difference method is shown in Figure 15. The maximum spectrum is normalized to 0 decibels. Those below -50 are set to zero and those higher or equal to -25 decibels are represented by X. The asterick (*) represents the lowest and the next lowest points of the spectrum. The solid curve connecting the low points in the trough is the phase velocity dispersion curve. There are several possible curves in this diagram. This one is chosen because the phase velocities associated with this curve are similar to those found by the peak-and-trough method.

C. Computing Phase Velocity Dispersion Curve by Using the Knowledge of Observational Group Velocities

The use of this method is two-fold. Firstly, it may be used to check the correctness of the results obtained by other methods. Secondly, the results of this method is expected to be less scattered because the group velocity dispersion curve, obtained by the moving window spectral analysis method, is relatively smooth.

Equation (2.7), which relates the phase velocity to the group velocity, is a first order differential equation. The numerical technique used to solve it is the Runge-Kutta method of order 4 (Conte, 1965). The details of this method is given in Appendix A. The group velocity data are those from the moving window spectral analysis method.

The disadvantage of this method is that an initial value

0	-47.5 DB AND BELOW	X	MINIMA AND NEXT MINIMA
1	-47.5 DB TO -45 DB	--	PHASE VELOCITY DISPERSION
9	-27.5 DB TO - 25 DB	INCREMENT OF NUMBERS : 0,1,2,3,4,5,6,7,	
X	-25 DB AND ABOVE	8, AND 9 = 2.5 DB	

FIGURE 15. PHASE VELOCITY DISPERSION CURVE OBTAINED BY FOURIER SUM-AND-DIFFERENCE METHOD(RECORD #43, 2ND & 6TH TRACES)

of phase velocity is needed before the computation can start. This is probably one of the reasons that, to the author's knowledge, this method has not been used previously. Another reason may be that before the development of the moving window spectral analysis method by Landisman, et al (1969), the observational group velocity data is quite scattered and not suitable for using this method. To find a good initial value, one could resort to the results obtained from the Fourier sum-and-difference method. Two examples of the results using this method are tabulated in Tables 4a and 4b. The closeness between the Fourier sum-and-error method and this method verifies the success of these two methods.

Table 4a. Phase Velocities Obtained by Integrating Observational Group Velocity Dispersion Curve (Record No. 43 second ℞ trace)

Group Velocity (ft/sec)	Frequency (cps)	Phase Velocity (ft/sec)	Phase Velocity *Difference
569.444	8.50	# 740.741	0.000
559.345	8.75		
550.336	9.00	727.643	0.370
542.328	9.25		
534.550	9.50	714.788	0.502
524.297	9.75		
514.429	10.00	702.035	0.281
488.677	10.25		
482.921	10.50	688.029	-1.626
478.972	10.75		
475.638	11.00	674.653	?
474.537	11.25		
473.441	11.50	662.506	?
470.723	11.75		
468.571	12.00	651.454	-4.284
465.909	12.25		
463.801	12.50	641.246	?
461.712	12.75		
460.157	13.00	631.804	-3.117
456.062	13.25		
452.539	13.50	622.919	?
449.069	13.75		
445.652	14.00	614.424	-0.961

*Phase velocity obtained by integration — Phase velocity obtained by Fourier sum-and-difference method.
#This is an initial value selected from the phase velocities obtained by Fourier sum-and-difference method.
?Difficult to determine the correct phase velocity corresponding to this frequency.

Table 4b. Phase Velocities Obtained by Integrating Observational Group Velocity Dispersion (Record No. 43, Sixth Z trace)

Group Velocity (ft/sec)	Frequency (cps)	Phase Velocity (ft/sec)	Phase Velocity *Difference
572.519	8.50	# 740.741	0.000
563.910	8.75		
554.871	9.00	728.047	0.774
547.445	9.25		
540.216	9.50	715.621	1 335
533.175	9.75		
526.932	10.00	703.592	1.838
502.793	10.25		
498.339	10.50	690.739	1.084
487.013	10.75		
482.315	11.00	677.943	?
477.707	11.25		
473.186	11.50	665.809	?
470.711	11.75		
468.262	12.00	654.506	-1.232
466.321	12.25		
464.396	12.50	644.109	?
461.066	12.75		
457.317	13.00	634.416	-0.505

* Phase velocity obtained by integration — (Minus) Phase velocity obtained by Fourier sum-and-difference method.

\# This is an initial value selected from the phase velocities obtained by Fourier sum-and-difference method.

? Difficult to determine the correct phase velocity corresponding to this frequency.

Chapter V
Inversion of Data to Yield Model Parameters

In this chapter, various methods of inverting observational data and the resulting model parameters will be discussed. The emphasis will be placed upon the inversion of normal modes. A comparison of the results determined by normal mode, leaking mode, and compressional wave data will be made in the last section.

A. Inversion of Normal Mode Data

The observational phase velocities obtained in Chapter IV are the data used in the inversion of normal modes. The period equation which relates the phase velocity data to the model parameters is equation (2.8).

1. Methods

Equation (2.8) has long been used in generating theoretical dispersion patterns corresponding to assumed crust-mantle models. These dispersion patterns are used in comparison with the earthquake surface wave data and to test the correctness of the assumptions. For a layer over a half-space model, there are six model parameters of which one could speculate. By a trial-and-error method, it is possible to get an estimate, but of course, uncertainty remains. Dorman and Ewing (1962) were the first to inverse the observational phase velocities directly without assuming model parameters. They used the linear least-square approach.

Two new methods have been developed here to find the model parameters directly from the observational phase velocities. Because these two methods were developed independently, without the knowledge of Dorman and Ewing (1962), any comparison was not intended.

a. Exact Method

Six model parameters, P wave velocities in the surface layer and in the half-space, S wave velocities in the surface layer and in the half-space, rigidity ratio of the two layers, and thickness of the surface layer uniquely determine the dispersion curves of all the leaking and normal modes corresponding to the single surface layer model. Conversely, these dispersion curves uniquely determine the six model parameters. The first step of the exact method is to arbitrarily choose six phase velocity-frequency pairs from any one or more dispersion curves. The second step is to solve for the six model parameter, from the six independent equations formed by substituting the six phase velocity-frequency pairs into the period equation.

If the observational phase velocity data were used, the inverted model parameters would not be correct, due to the observational errors. A method of solving this problem is to repeat this process for many times using different combinations of phase velocity-frequency pairs. According to the author's experience, the phase velocity data obtained by the integration of the group velocities give model parameters with relatively small errors. The final results are obtained

by averaging the results from different trials.

The numerical method used in solving these equations is Newton's method for a system of non-linear equations (Conte, 1965). The details of this method is given in Appendix B. This method converges fast when the initial values are chosen close enough to the true roots. If the initial values are out of range it may either converge to incorrect roots or not converge at all. Also, some of the results obtained by using the arbitrarily chosen phase velocity-frequency pairs, may deviate greatly from the optimal solution using the entire data set, if these chosen data points happen to contain greater observational errors. A careful inspection of the results from each trial must be undertaken and the far different solutions must be excluded before the averaging process is made. Some of the trials may not converge at all because of the vanishing Jacobian (Conte, 1965, p. 45). The numerical instability is caused by an inadequate combination of phase velocity-frequency pairs.

Two model parameters, the P wave velocities in the surface layer and in the half-space, are relatively well determined in this study. They are assigned 1150 and 5700 ft/sec, respectively. Therefore, only four unknowns enter the problem in the single surface layer model. An example of results obtained by the inversion of M_{11} data are listed in Table 5. The density ratio was computed by using the relation:

Table 5. Model Parameters Obtained by the Inversion of M_{11} Data Through the Use of the Exact Method (Record No. 43, Second Z trace)

	Mean Value	Standard Deviation	Percentage Error
Rigidity Ratio	2.26	0.27	±11.78
Thickness of Surface Layer (ft)	21.84	1.35	± 6.19
S Wave Velocity in Surface Layer (ft/sec)	603.31	7.61	± 1.26
S Wave Velocity in Half-Space (ft/sec)	904.03	25.67	± 2.84
Density Ratio	1.02	0.21	±20.30
Poisson's Ratio (Surface Layer)	0.30	----	----
Poisson's Ratio (Half-space)	0.49	----	----

Remarks:
i) 20 total data sets are inverted.
ii) only 12 sets of the inverted results are considered to be good and averaged to yield the mean values.

$$\text{Density Ratio} = \frac{\text{Density of Half-space Material}}{\text{Density of Surface Layer Material}} = \frac{\rho_2}{\rho_1}$$

$$= \left(\frac{\text{S Wave Velocity in Surface Layer}}{\text{S Wave Velocity in Half-space}}\right)^2 \times$$

Rigidity Ratio,

where the rigidity ratio is defined as:

$$\frac{\text{Rigidity of Half-space Material}}{\text{Rigidity of Surface Layer Material}} = \frac{\mu_2}{\mu_1}.$$

And, the Poisson's Ratios were found by the formula:

$$\text{Poisson's Ratio} = \frac{1}{2}\ \frac{\alpha^2 - 2\beta^2}{\alpha^2 - \beta^2}$$

where α = P wave velocity

β = S wave velocity.

These equations can be easily derived by using the relationships between body waves and elastic constants (Grant and West, 1968, p. 30).

b. Method by Minimizing Sum of Squared Residues

Instead of solving n equation with n unknowns, as does the method described in the preceeding section, a method which finds the optimal solutions to m equations in n unknowns for m > n, will be introduced here. This method is

similar to the well-known linear least-square technique, except that the equations are non-linear and the mathematical method in solving these equations is also non-linear.

The details of this method are as follows: Suppose that m observational phase velocity-frequency pairs are available for use in inversion. By substituting them into equation (2.8) and assuming n unknown model parameters, a system of m independent equations results:

$$\begin{aligned} f_1(a_1, a_2, \ldots, a_n) &= r_1 \\ f_2(a_1, a_2, \ldots, a_n) &= r_2 \qquad \ldots\ldots\ldots\ldots\ldots\ldots\ldots\ldots \quad (5.1) \\ &\vdots \\ f_m(a_1, a_2, \ldots, a_n) &= r_m \end{aligned}$$

where f_i's are period equations formed by substituting different phase velocity-frequency pairs, r_i's are residues of the equations due to the errors in the observational data ($i=1,2,\ldots,m$), and a_L's are model parameters to be determined ($L=1,2,\ldots,n$). A method of solving this system is to reduce the m equations to become n new equations in n unknowns by minimizing the sum of squared residues, r_i's ; and then solving the new system exactly. Namely, the a_L parameters are to be solved subject to the constraint:

$$\sum_{i=1}^{m} r_i = \text{minimum}$$

or

$$\sum_{i=1}^{m} f_i^2 = \text{minimum} \qquad (5.2)$$

Differentiating equation (5.2) with respect to a_L's , one obtains

$$\begin{aligned}
2 \sum_{i=1}^{m} f_i \frac{\partial f_i}{\partial a_1} &= 0 \\
2 \sum_{i=1}^{m} f_i \frac{\partial f_i}{\partial a_2} &= 0 \qquad (5.3) \\
2 \sum_{i=1}^{m} f_i \frac{\partial f_i}{\partial a_3} &= 0 \\
&\vdots \\
2 \sum_{i=1}^{m} f_i \frac{\partial f_i}{\partial a_n} &= 0 .
\end{aligned}$$

Equation (5.3) is a system of n non-linear equations in n unknowns. It can be solved by numerical methods. If the input data were not independently observed this method might not be valid. Also, this kind of minimization process may not be valid for some particular mathematic functions. These mathematical problems will not be theoretically treated here. The closeness of the results by using this method and the one described in the preceeding section is evidence that this is a good method for our particular data and particular period equation.

Some details of solving equation (5.3) by using the

Newton's method for a system of non-linear equation are given here. Define:

$$G_1(a_1, a_2, \ldots, a_n) = \sum_{i=1}^{m} f_i \frac{\partial f_i}{\partial a_1}$$

$$G_2(a_1, a_2, \ldots, a_n) = \sum_{i=1}^{m} f_i \frac{\partial f_i}{\partial a_2} \quad \ldots\ldots\ldots\ldots\ldots\ldots \quad (5.4)$$

$$\vdots$$

$$G_n(a_1, a_2, \ldots, a_n) = \sum_{i=1}^{m} f_i \frac{\partial f_i}{\partial a_n}.$$

The iteration scheme of the Newton's method is:

$$(a_k)_{P+1} = (a_k)_P + N/D, \quad \ldots\ldots\ldots\ldots\ldots\ldots\ldots\ldots \quad (5.5)$$

where

$k = 1, 2, 2, \ldots, n$

P = number of iterations

$$N = \begin{vmatrix} \frac{\partial G_1}{\partial a_1} & \frac{\partial G_1}{\partial a_2} & \cdots & \frac{\partial G_1}{\partial a_{k-1}} & -G_1 & \frac{\partial G_1}{\partial a_{k+1}} & \cdots & \frac{\partial G_1}{\partial a_n} \\ \frac{\partial G_2}{\partial a_1} & \frac{\partial G_2}{\partial a_2} & \cdots & \frac{\partial G_2}{\partial a_{k-1}} & -G_2 & \frac{\partial G_2}{\partial a_{k+1}} & \cdots & \frac{\partial G_2}{\partial a_n} \\ \vdots & \vdots & & \vdots & \vdots & \vdots & & \vdots \\ \frac{\partial G_n}{\partial a_1} & \frac{\partial G_n}{\partial a_2} & \cdots & \frac{\partial G_n}{\partial a_{k-1}} & -G_n & \frac{\partial G_n}{\partial a_{k+1}} & \cdots & \frac{\partial G_n}{\partial a_n} \end{vmatrix}$$

$$D = \begin{vmatrix} \frac{\partial G_1}{\partial a_1} & \frac{\partial G_1}{\partial a_2} & \cdots & \frac{\partial G_1}{\partial a_n} \\ \frac{\partial G_2}{\partial a_1} & \frac{\partial G_2}{\partial a_2} & \cdots & \frac{\partial G_2}{\partial a_n} \\ \vdots & \vdots & & \vdots \\ \frac{\partial G_n}{\partial a_1} & \frac{\partial G_n}{\partial a_2} & \cdots & \frac{\partial G_n}{\partial a_n} \end{vmatrix} = \text{Jacobian}$$

The major difficulty of this method is that the second derivatives of equation (2.8) with respect to each parameter are required in programming. The derivative

$$\frac{\partial G_i}{\partial a_k} = \frac{\partial}{\partial a_k} \sum_{l=1}^{m} f_l \frac{\partial f_l}{\partial a_i} = \sum_{l=1}^{m} \left[\frac{\partial f_l}{\partial a_k} \frac{\partial f_l}{\partial a_i} + f_l \frac{\partial^2 f_l}{\partial a_k \partial a_i} \right]$$

is an example.

Although the programming of this method is laborious, the computer time needed in computation is surprisingly small and the results are close to those obtained in preceeding sections. The model parameters computed by this method are listed in Table 6. The S wave velocity in the surface layer was not computed by this method. Because the value 603.3 ft/sec found by the exact method in previouu section is very close to the value 600 ft/sec determined by Bennett (1973), it was thought that these two values must be close enough to the true value.

Table 6. Model Parameters Obtained by the Inversion of M_{11} Data Through the Use of the Method of Minimizing Sum of Squared Residues (Record No. 43, Z component)

	Second Trace	Sixth Trace
Rigidity Ratio	2.26	2.17
Thickness (Surface Layer)	21.95	21.34
S velocity (Half-space)	902.00	902.47
Density Ratio	1.01	0.97
Poisson's Ratio (Surface Layer)	0.31	0.31
Poisson's Ratio (Half-space)	0.49	0.49

2. Checking the Correctness of Inverted Model Parameters by Reversing Process

The best method of checking the correctness of the inverted model parameters is to reverse the process and to check the differences between these dispersion curves obtained by the reverse process and the observational dispersion curves. The reverse process is just the traditional method of deriving theoretical phase and group velocity dispersion curves (Ewing, et al, 1957). The details are given in Appendix C.

Table 7 shows a comparison of the theoretical and the observational phase and group velocity dispersion curves. The same data is plotted in Figure 16.

B. A Discussion of the Model Parameters Derived From Normal Mode, Leaking Mode, and Compressional Wave Data

The P wave velocity in the surface layer has not been computed in the study due to the difficulty in determining the accurate times of the direct P wave arrivals. The value of 1150 ft/sec has been used throughout the study. It was determined by Bennett (1973) using short distance refraction surveys. In his study it was also found that a low velocity loose sand with variable thickness was present near the free surface.

The P wave velocity in the saturated layer was computed by the standard refraction time-distance curves to be 5700 ft/sec. This velocity and the P wave velocity in the Mississippian sandstone, which was found by the same method,

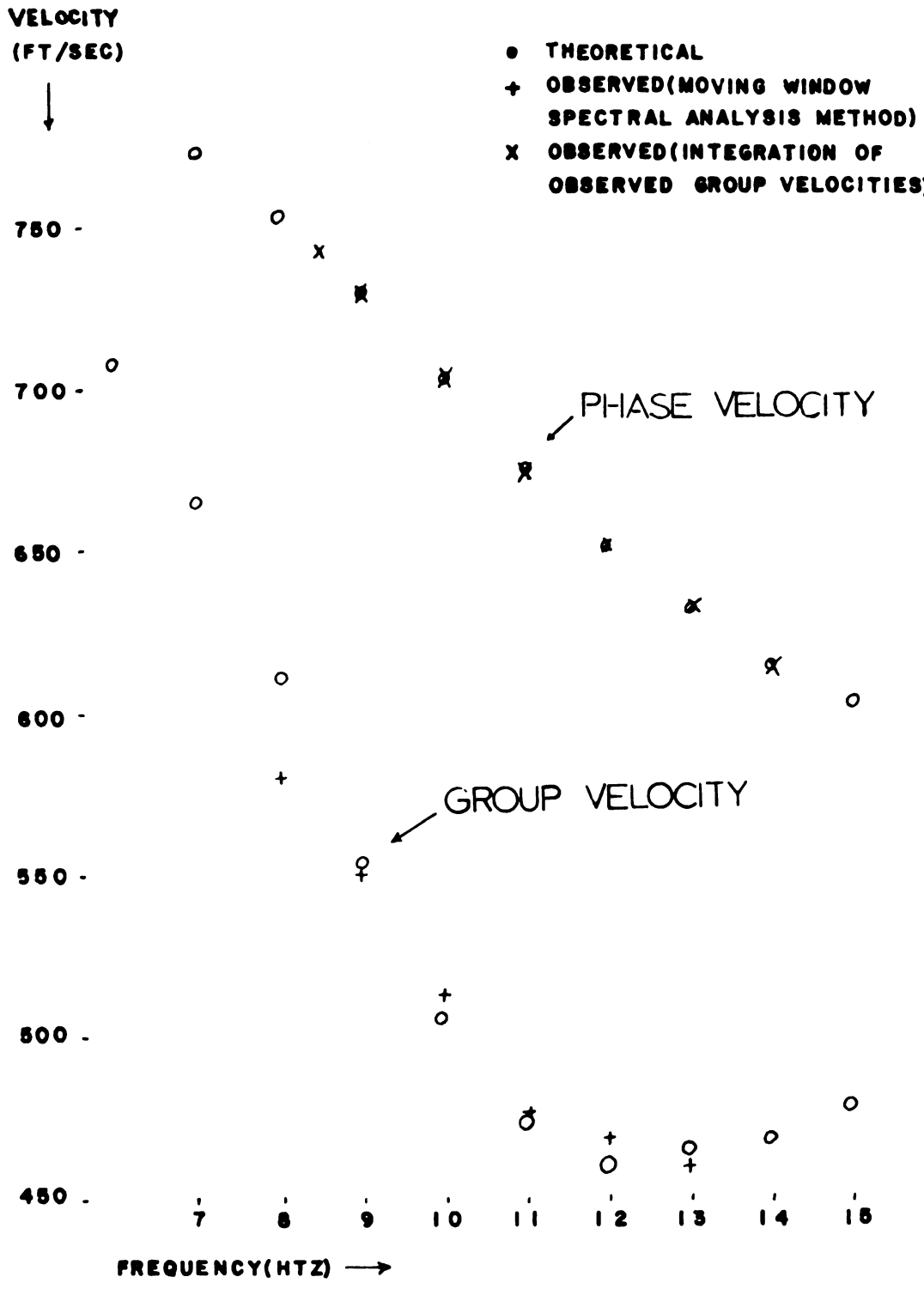

FIGURE 16. OBSERVED AND THEORETICAL DISPERSION OF M_{11} MODE

Table 7. A Comparison of the Theoretical and the Observational Phase and Group Velocity Dispersion
(M_{11} data taken from Record No. 43, second Z trace)

Frequency (HTZ)	Phase Velocity (Ft/sec)	*Phase Velocity Difference	Group Velocity (Ft/sec)	#Group Velocity Difference
8.50	740.6087	-0.1323	582.5392	13.0952
9.00	728.3312	0.7878	554.3113	3.9753
9.50	715.2862	0.4978	528.1900	-6.3600
10.00	701.7815	-0.2535	505.6809	-8.7481
10.50	688.2109	0.1815	487.8027	4.8817
11.00	674.9856	0.3324	474.8996	-0.7384
11.50	662.4602	-0.0458	466.6908	-6.7502
12.00	650.8844	-0.5699	462.4858	-6.0852
12.50	640.3907	-0.8555	461.4311	-2.3699
13.00	631.0123	-0.7912	467.6952	-2.5382
13.50	622.7123	-0.2058	465.5661	13.0571
14.00	615.4122	0.9882	469.4813	23.8293

* Theoretical phase velocity minus Observational Phase velocity (by integration of group velocities).

\# Theoretical group velocity minus Observational Group velocity (by moving window spectral analysis method).

are believed to be reliable because both arriving times are accurately determined in the study.

The S wave velocity in the surface layer has been determined to be 603 ft/sec by the inversion of the M_{11} data. It is surprisingly close to the value 550 to 600 ft/sec, which was measured by Bennett (1973) using hammer blows as sources and at short distances less than 100 ft.

It was also computed, by using M_{11} data, that the S wave velocity in the half-space of the single surface layer model is 902 ft/sec. It is different from the value of 1200 ft/sec for the saturated layer by Bennett (1973). In Chapter II other evidences that support the existence of the layer with 902 ft/sec, have been discussed. Having been mentioned before, the clay layers in the Pleistocene glacial drift are possible of causing larger shear wave velocity changes than the water-table.

The driller's well log indicates that the depth to the water-table is about 32 ft (Todd, 1971). By applying the standard refraction technique, it was found to be 46 ft in Record No. 43, 41 ft on Record No. 10. Todd (1971) identified eight successive multiple reflections right after the refracted P wave from the saturated layer and found the average time lag between two sequential reflections to be 0.056 sec. The depth corresponding to this value is 33 ft. After examining his record, the first time lag, i.e., the one between the refracted P wave and the first reflection, has a stable value of about 0.060 sec. This is equivalent

to a depth of 35 ft. It is felt that the first time lag rather than the average value must be used in the calculation. However, the depth, based upon the first time lag, seems to be more in error as compared to the one based upon the average time lag. The low velocity material right near the surface and the elongated ray path due to velocity gradient may cause this discrepancy. By using the first time lag, the depths are determined to be 41 ft on Record No. 43, 36 ft on Record No. 33, and 33 ft on Record No. 10. The depth can also be determined from the spectra of the "pipe organ" modes. The first three modes have peak amplitude spectra at 10.000, 23.333, and 35.000 cps in Record No. 43, 10.667, 26.667, and 42.667 cps in Record No. 33, and 11.429, 23.143, and 44.286 cps in Record No. 10. The true "pipe organ" modes are supposed to peak at frequencies with ratios of 1, 3, 5, 7, ... The departure of the observed ones from the true "pipe organ" modes has been discussed in some detail in Chapter II. Since these modes are dispersive, their frequencies actually vary with time. The frequencies of the true "pipe organ" modes as their phase velocities approach the P wave velocity of the saturated layer. The fundamental frequencies of the true "pipe organ" modes, derived under this requirement from the observed data, are 7.000 cps for Record No. 43, 8.533 cps for Record No. 33, and 8.857 cps for Record No. 10. These frequencies are equivalent to depths of 41.9 ft for Record No. 43, 34.4 ft for record No. 33, and 32.5 ft for Record No. 10. The depths to the water-

table computed by various methods are summarized in Table 8. The shot-receiver distances and geophone spacings of the records used can be found in Table 2, p. 51.

It is observed that the depths based upon the first reflection and "pipe organ" mode data are very close. Although the exact depths at each station are not known, it is believed that these two sets of values are slightly higher than the true values. The small positive errors are due to the low velocity material near free surface and the elongated ray paths caused by the velocity gradient. The depths determined from the refracted P wave are obviously in error. The intercept times used in computing the depths are obtained by extending the time-distance curves to intercept the time axis. The range of a T-D curve, that is actually determined from the observed data, is limited by the spread of the geophone array, which is small as compared to the shot-receive distance for the records studied. The extension of a T-D curve to intercept the time axis is inevitably subject to error. The depths found by using record No. 43 data are greater than those found by using other records. This may be due to the descending of the water-table because the recording site of No. 43 is farther from the source of the ground water than the recording sites of other records (personal communication with Dr. H. F. Bennett of the Department of Geology).

The thickness of the surface layer of the single surface layer model, computed from the M_{11} data of record No. 43, is

Table 8. The Depths to the Water-table

Data Based	*Refracted P Wave			*First Reflection			# "Pipe Organ" Mode		
Record Number	10	33	43	10	33	43	10	33	43
Depth (ft)	41.0	?	48.0	33.0	35.7	41.0	32.5	34.4	41.9

? Difficult to measure the slope of the time-distance curve

* All traces in Z component were used in computation

Z component traces used in computation are: Record No. 10---4th and 7th, Record No. 33---1st, 2nd and 3rd, Record No. 43---2nd and 6th, Record No. 42 (results included in No. 43) ---1st, 4th and 7th

about 22 ft. This value is apparently not the depth to water-table. The original thinking is that because most seismic energy is trapped in the unsaturated layer above the water-table, the W-T may act as the interface of the assumed surface wave model. By re-examining the techniques used in studying surface waves, no problems that may introduce errors have been found. In the same evaluation, the S wave velocity of the surface layer which has been mentioned previously, is verified to be correct and the density ratio at the interface is about 1.0. This indicates that it is not an unsaturated-saturated boundary because the porosity of the glacial sand in this area is about 25% (Bennett, 1973) and the corresponding density ratio at the W-T is about 1.1. It has been well established that the normal modes are several times more sensitive to the S wave velocity distribution than the leaking modes. On the other hand, the leaking modes are more sensitive to the P wave velocity distribution (Su and Dorman, 1965, pp. 1008-1009). It is logical to accept the fact that a S wave velocity discontinuity exists at a depth of 22 ft. This discontinuity may be a result of lithology change (clay layer), compaction, or cementation. Unfortunately, this result does not contribute anything to the controversial problem discussed in Chapter II: Does the S wave velocity change at the water-table or not? One possible inference is that the S wave velocity change at W-T is of a magnitude less than the one at the level of

22 ft, where the velocity increases from 603 ft/sec to 902 ft/sec. If a multi-layered medium is assumed to be a single layer over a half-space model in surface wave inversion, the interface of the model will be found at the level where the maximum change in S wave velocity occurs. That is because the dispersion pattern of the model, using this level as the interface, is close to the actual dispersion pattern of the multi-layered medium.

Chapter VI
Summary and Conclusions

This study has been centering around the problem of the utilization of leaking and normal modes from a small explosion. The difficulties of this problem result from the presence of a high level of noise, an immaturely developed wave form, and a short time duration of the signal. The emphasis of the study has been placed upon the use of numerical techniques to achieve better results. Some problems pertaining to the theory, and the particular data used, have also been studied.

A. Numerical Techniques

All the numerical techniques used in the study have been carefully examined. To check the correctness of the results of a newly developed or modified technique, one or more other methods were used to the same set of data, and a comparison was made. In some cases, the testing of techniques was made by reversing the process. Because of these careful considerations, the techniques used in the study are believed to be reliable. This study may be helpful for other workers who wish to study the seismic data of similar nature by numerical techniques.

1. Derivation of Time-varying Spectra and Group Velocities

A special version of the moving window spectral analy-

sis method has been proved to be an effective means of separating superimposed modes and identifying signals. The group velocity dispersion curves derived by this method are smoother than those derived by the traditional, visual measurement of periods. To save computer time, an approximation method of the one-period Fourier transform was developed, and Page's (1952) instantaneous power spectrum was implemented in the moving window spectral analysis method.

2. Computation of Phase Velocities

Some methods were found to give poor results using the available data. The Fourier sum-and-difference method using the time-varying filtered data gives a good dispersion curve. This method uses the shift of the time origin of one seismic trace with respect to another. By using a trapezoidal window, and doing the time shifting in the frequency domain instead of the time domain, two advantages result. One is the reduction of time needed in performing Fourier transform. Another is that no additional noises are introduced. The derivation of phase velocities from the observational group velocity dispersion curves yields smooth phase velocity dispersion curves suitable for the inversion computation.

3. Inversion Methods

The exact method for the inversion of the phase velocities to yield model parameters is easy to apply. The method of minimizing the sum of squared residues is difficult

in programming, but the computer time needed is small. The results of these two methods were compared and a good agreement was found. To further assure their correctness, the inverted model parameters were used to compute the theoretical dispersion curves, and then compared to the observational ones. The differences between the theoretical, and the observational ones are small. There are larger deviations in group velocities at low and high frequencies. The higher degree of uncertainty in determining the correct values at the two ends of the observational group velocity dispersion curve may be the source of errors.

B. The Use of Normal and Leaking Modes in Data Interpretation

In all the records studied, M_{11} mode has the most well developed wave form. For shot-receiver distance less than 1000 ft, the time duration of this mode is still too short for the accurate phase velocity dispersion curve to be easily determined. This is why only the results, computed from the M_{11} data in record No. 43 are shown in previous chapters. The M_{12} and M_{21} data may be possible to utilize when the shot-receiver distance is longer than 2000 ft. The use of normal modes not only gives an independent check on the results obtained by using body wave data, but also gives lithological information.

The dispersive "pipe organ" modes found in the data studied, can be used to find the depth to the water-table. The results agree with those obtained by using the time

lags between the refracted P wave and the first reflection. The depth determined from the "pipe organ" modes may be more reliable than the ones determined from the refracted P wave arrivals when shot-receiver distance is large as compared to the spread of the geophone array. A theoretical derivation was made in Chapter II to show the possible existence of the dispersive "pipe organ" modes in the unsaturated layer overlying the saturated half-space. This theoretical treatment was not done in rigorous manner. An actual numerical calculation must be made and more observational data must be collected to verify its correctness. If the dispersive "pipe organ" modes are verified to appear only in this particular situation, their appearance will be a good indication of the existence of a water-table.

In the assumed model, the boundary with large S wave velocity change becomes the interface of the model for normal modes, and the boundary with large P wave velocity change becomes the interface of the model for leaking modes. This is in agreement with the conclusions of Su and Dorman (1965). In this study the S wave velocity change at the water-table was not detectable. This does not exclude the existence of this velocity discontinuity.

In future study, the Haskell's matrix must be used in the surface wave computation. It is more flexible in shifting from the single-layered half-space model to the multi-layered model. A more accurate result may be

obtained.

C. Miscellaneous Conclusions and Recommendations

In addition to the conclusions of Tolstoy and Usdin (1953) regarding the existence of the symmetric and anti-symmetric modes in a solid layer overlying a solid half-space model, a theoretical derivation was made to prove that they exist under all conditions.

Only X and Z components of the records have been carefully studied. The spectra of the Y component was only lightly studied. It was found that the spectral properties of the Y component are different from X and Z components. This is because the theory underlying the SH motions of the Y component is independent from the one for the other two components. Additional information may be obtained through the study of this component.

Although linear filters are not suitable for studying dispersive wave trains, they are recommended for use in the detection of direct, refracted, and reflected body wave arrivals and to add more information to the study.

A P P E N D I C E S

Appendix A. Runge-Kutta Method of Order 4 Used in Computing Phase Velocities

The problem here is to solve a first order ordinary differential equation of the form

$$\frac{dC(f)}{df} = \frac{C(f)}{fU(f)} [U(f) - C(f)] = F(f,C) \quad \ldots\ldots\ldots\ldots \text{(A1)}$$

with initial condition

$C(f_o) = C_o$

where C = Phase velocity

U = Group velocity (an implicit function of f)

f = Frequency

fo = Initial value of f

Co = Initial value of C.

In computer computation a value observed on the observational group velocity dispersion curve is substituted for U. Co is a phase velocity chosen from the results of Fourier sum-and-difference method. Note that equation (A-1) is the same as equation (2.7). Here, $w = w_a$ and $C = C_a$ are understood.

The recursion formula for numerical computation is: (Conte, 1965, p. 223) $C_{n+1} = C_n + 1/6\ (K_1 + 2K_2 + 2K_3 + K_4)$

where $K_1 = h\ F\ (fn, Cn)$

$K_2 = h\ F\ (fn + h/2, Cn + 1/2\ K_1)$

$K_3 = h\ F\ (fn + h/2, Cn + 1/2\ K_2)$

$K_4 = h\ F\ (fn + h, Cn + K_3)$

$n = 0, 1, 2, \ldots$ = Iteration step

h = Step size of frequency.

Appendix B. Newton's Method for Simultaneous Non-Linear Equations

The simultaneous non-linear equations

$$F_1 (X_1, X_2, \ldots X_n) = 0$$

$$F_2 (X_1, X_2, \ldots X_n) = 0$$

$$\vdots$$

$$F_n (X_1, X_2, \ldots X_n) = 0$$

are to be solved. Assuming that $F_1, F_2, \ldots F_n$ and all their derivatives through second order are continuous and bounded in a region containing the true solutions $(A_1, A_2, \ldots, A_n)$ and the initial approximation $(a_1, a_2, a_3, \ldots, a_n)$ is chosen sufficiently close to $(A_1, A_2, \ldots, A_n)$. By expanding $F_1, F_2, \ldots F_n$ about $(a_1, a_2, \ldots, a_n)$, one gets

$$F_1 (X_1, X_2, \ldots, X_n) = F_1(a_1, a_2, \ldots, a_n)$$

$$+$$

$$\frac{\partial F_1(a_1, a_2, \ldots, a_n)}{\partial X_1} (X_1-a_1)$$

$$+$$

$$\frac{\partial F_1(a_1, a_2, \ldots, a_n)}{\partial X_2} (X_2-a_2) + \ldots \frac{\partial F_1(a_1, a_2, \ldots, a_n)}{\partial X_n} (X_n-a_n)$$

$$+ \text{ Higher-order Terms}$$

$$F_2 (X_1, X_2, \ldots, X_n) = F_2(a_1,a_2, \ldots, a_n) + \frac{\partial F_2(a_1,a_2, \ldots, a_n)}{\partial X_1} \cdot (X_1-a_1)$$

$$+ \frac{\partial F_2(a_1, a_2, \ldots, a_n)}{\partial x_2} (X_2 - a_2) + \text{------}$$

$$+ \frac{\partial F_2(a_1, a_2, \ldots, a_n)}{\partial X_n} (X_n - a_n)$$

+ Higher-order Terms

$$\vdots$$

$$F_n(X_1, X_2, \ldots, X_n) = F_n(a_1, a_2, \ldots, a_n)$$

$$+ \frac{\partial F_n(a_1, a_2, \ldots, a_n)}{\partial X_1} (X_1 - a_1)$$

$$+ \frac{\partial F_n(a_1, a_2, \ldots, a_n)}{\partial X_2} (X_2 - a_2) + \text{---}$$

$$+ \frac{\partial F(a_1, a_2, \ldots, a_n)}{\partial X_n} (X_n - a_n)$$

+ Higher-order Terms.

By neglecting the higher-order terms, the above equations can be written as:

$$\frac{\partial F_1}{\partial X_1}(X_1 - a_1) + \frac{\partial F_1}{\partial X_2}(X_2 - a_2) + \text{---} + \frac{\partial F_1}{\partial X_n}(X_n - a_n) = -F_1$$

$$\frac{\partial F_2}{\partial X_1}(X_1 - a_1) + \frac{\partial F_2}{\partial X_2}(X_2 - a_2) + \text{---} + \frac{\partial F_2}{\partial X_n}(X_n - a_n) = -F_2$$

$$\vdots$$

$$\frac{\partial F_n}{\partial X_1}(X_1 - a_1) + \frac{\partial F_n}{\partial X_2}(X_2 - a_2) + \text{---} + \frac{\partial F_n}{\partial X_n}(X_n - a_n) = -F_n$$

Therefore, a recursion formula is: (Conte, 1965, pp. 45-46)

$$a_{1,i+1} = a_{1,i} + \frac{\begin{vmatrix} -F_1 & \frac{\partial F_1}{\partial X_2} & \cdots & \frac{\partial F_1}{\partial X_n} \\ \vdots & \vdots & & \vdots \\ -F_n & \frac{\partial F_n}{\partial X_2} & \cdots & \frac{\partial F_n}{\partial X_n} \end{vmatrix}}{J(F_1, F_2, \cdots, F_n)} \qquad X_l = a_{l,i} \quad l = 1, 2, \cdots, n$$

$$a_{2,i+1} = a_{2,i} + \frac{\begin{vmatrix} \frac{\partial F_1}{\partial X_1} & -F_1 & \frac{\partial F_1}{\partial X_3} & \cdots & \frac{\partial F_1}{\partial X_n} \\ \vdots & \vdots & \vdots & & \vdots \\ \frac{\partial F_n}{\partial X_1} & -F_n & \frac{\partial F_n}{\partial X_3} & \cdots & \frac{\partial F_n}{\partial X_n} \end{vmatrix}}{J(F_1, F_2, \cdots, F_n)} \qquad X_l = a_{l,i} \quad l = 1, 2, \cdots, n$$

$$a_{n,i+1} = a_{n,i} + \frac{\begin{vmatrix} \frac{\partial F_1}{\partial X_1} & \frac{\partial F_1}{\partial X_2} & \cdots & -F_1 \\ \vdots & \vdots & & \vdots \\ \frac{\partial F_n}{\partial X_1} & \frac{\partial F_n}{\partial X_2} & \cdots & -F_n \end{vmatrix}}{J(F_1, F_2, \cdots, F_n)} \qquad X_l = a_{l,i} \quad l = 1, 2, \cdots, n$$

where

$$J(F_1, F_2, \cdots, F_n) = \begin{vmatrix} \frac{\partial F_1}{\partial X_1} & \frac{\partial F_1}{\partial X_2} & \cdots & \frac{\partial F_1}{\partial X_n} \\ \vdots & & & \vdots \\ \frac{\partial F_n}{\partial X_1} & \frac{\partial F_n}{\partial X_2} & \cdots & \frac{\partial F_n}{\partial X_n} \end{vmatrix} = \text{Jacobian} \neq 0$$

i = number of iterations.

Appendix C. Numerical Methods of Computing Theoretical Dispersion Curves

The period equation of a solid surface layer overlying a solid half-space, equation (2.8), is used in the computations herein. For $\beta_1 < C \leq \beta_2$, the real solutions of this equation exist and represent the unattenuated propagation. The existence of the real solutions is not affected by

$$\alpha_1 > \beta_2 \qquad \text{or} \qquad \alpha_1 < \beta_2 \ .$$

To derive the phase velocity dispersion curves, the Newton's method is used. An initial value of phase velocity Co must be estimated at the beginning. The iteration scheme is: (Conte, 1965, p. 31)

$$C_{i+1} = C_i - \left(P(C, f_a) \Big/ \frac{\partial P(C, f_a)}{\partial C} \right)_i$$

where $i = 0, 1, 2, \ldots$ = number of iterations

$P(C, f_a)$ is the period function in equation (2.8)

f_a is a particular frequency of interest.

The iteration stops when the successive values differ by less than 10^{-7} . The estimated value of C for $f_b = f_a + \Delta f$, where Δf is a finite increment of frequency, is derived as follows: Denote the period equation (2.8) by

$P(C,k) = o$ ..... (A2)

where $k = w/C$ = wave number

$w = 2\pi f = 2\pi X$ frequency,

By differentiating equation (A-2), yields:

$$dP(C,k) = \frac{\partial P}{\partial C} dC + \frac{\partial P}{\partial k} dk = o$$

or

$$\frac{dC}{dk} = - \left(\frac{\partial P}{\partial k}\right) / \left(\frac{\partial P}{\partial C}\right) \quad \text{..... (A3)}$$

Equation (A-3) can be rewritten as:

$$dC = -adk = -a \frac{2\pi}{C^2} (Cdf - fdC)$$

or

$$dC = -2\pi adf/(C-ak) \quad \text{..... (A4)}$$

where $a = \left(\frac{\partial P}{\partial k}\right) / \left(\frac{\partial P}{\partial C}\right)$.

An estimation of C at f_b can be found by an approximated version of equation (A-4) as follows:

$$(C)_{f=fb} = (C)_{f=fa} - [2\pi a \Delta f/(C-ak)]_{f = fa}.$$

To find group velocities from phase velocities, the following relationship is used:

$$U = C + k \frac{dC}{dk} \quad \text{- - - - - - - - - - - - - - - - - - (A 5)}$$

The direct numerical differentiation of C with respect to k often leads to significant errors. Mooney and Bolt (1966)

found that using equation (A 3) instead of direct numerical differentiation, a better result was achieved. Their method is used in our study.

R E F E R E N C E S

References

Alsop, L. E., 1970, The leaky-mode period equation---a plane wave approach, Bull. Seism. Soc. Am., v. 60, pp. 1989-1998.

Bennett, Hugh F., 1973, Application of seismic shear wave studies to the investigation of aquifers; Final report of the Department of Geology, Michigan State University.

Biot, M. A., 1956 a, Theory of propagation of elastic waves in a fluid-saturated porous solid; I: Low frequency range, Journ. Acoust. Soc. Am., v. 28, pp. 168-178.

____, 1956 b, Theory of propagation of elastic waves in a fluid-saturated porous solid; II: Higher frequency range, Journ. Acoust. Soc. Am., v. 28, pp. 179-191.

Bloch, S. and A. L. Hales, 1968, New techniques for the determination of surface wave phase velocities, Bull. Seism. Soc. Am., v. 58, pp. 1021-1034.

Conte, S. D., 1965, Elementary Numerical Analysis, McGraw-Hill Book Company, N.Y.

Dobrin, M. B., P. L. Lawrence, and R. L. Sengbush, 1954, Surface and near-surface waves in the Delaware Basin, Geophysics, v. 19, pp. 695-715.

Dorman, James and W. Maurice Ewing, 1962, Numerical inversion of surface wave dispersion data and crust-mantle structure in the New York-Pennsylvania area, J. Geophys. Res., v. 67, pp. 5227-5241.

Ewing, W. Maurice, W. S. Jardetzky, and F. Press, 1957, Elastic Waves in Layered Media, McGraw-Hill Book Company, New York.

Gilbert, F., 1964, Propagation of transient leaking modes in a stratified elastic wave guide, Rev. Geophys., v. 2, pp. 123-153.

Gold, B., and C. M. Rader, 1969, Digital Processing of Signals, McGraw-Hill Book Company, New York.

Grant, F. S. and G. F. West, 1968, Interpretation Theory in Applied Geophysics, McGraw-Hill Book Company, New York.

Haskell, N. A., 1953, The dispersion of surface waves in multi-layered media, Bull. Seism. Soc. Am., v. 43, pp. 17-34.

Hsu, Hwei P., 1970, Fourier Analysis, Simon and Schuster, New York.

Jenkins, G. M. and D. G. Watts, 1968, Spectral Analysis and its applications, Holden-Day, Inc., San Francisco.

Kisslinger, C., 1959, Observations of the development of Rayleigh-type waves in the vicinity of small explosions, J. Geophys. Res., v. 64, pp. 429-436.

Landisman, M., A. Dziewanski and Y. Satô, 1969, Recent improvements in the analysis of surface wave observations, Geophys. J. R. Soc., v. 17, pp. 369-403.

Mann, R. L., and I. Fatt, 1960, Effect of pore fluids on the elastic properties of sandstones, Geophysics, v. 25, pp. 433-444.

Mooney, H. M. and B. A. Bolt, 1966, Dispersive characteristics of the first three Rayleigh modes for a single surface layer, Bull. Seism. Soc. Am., v. 56, pp. 43-67.

Muskat, M., and M. W. Meres, 1950, Reflection and transmission coefficients for plane waves in elastic media, Geophysics, v. 5, pp. 115-148.

Officer, C. B., 1958, Introduction to the Theory of Sound Transmission, McGraw-Hill Book Company, New York.

Page, C. H., 1952, Instantaneous power spectra, J. App. Phys., v. 23, pp. 103-106.

Satô, Y., 1960, Analysis of surface waves in International Symposium on Stress Wave Propagation in Material, Interscience Publishers, Inc., New York, Norman Davids, Ed.

Su, S. S. and J. Dorman, 1965, The use of leaking modes in seismogram interpretation and in studies of crust-mantle structure, Bull. Seism. Soc. Am., v. 55, pp. 989-1021.

Todd, R. C., 1971, An investigation of the seismic wave propagation properties of a thin unsaturated layer as a wave guide. M. S. Thesis, Michigan State University.

Tolstoy, I. and E. Usdin, 1953, Dispersive properties of stratified elastic and liquid media: A ray theory, Geophysics, v. 18, pp. 844-870.

Watson, T. H., 1972, A real frequency, complex wave-number analysis of leaking modes, Bull. Seism. Soc. Am., v. 62, pp. 369-384.